Quantum quench of the Sachdev-Ye-Kitaev Model

Andreas Eberlein,[1] Valentin Kasper,[1] Subir Sachdev,[1,2] and Julia Steinberg[1]

[1] *Department of Physics, Harvard University, Cambridge, Massachusetts 02138, USA*

[2] *Perimeter Institute for Theoretical Physics, Waterloo, Ontario, Canada N2L 2Y5*

(Dated: September 24, 2017)

Abstract

We describe the non-equilibrium quench dynamics of the Sachdev-Ye-Kitaev models of fermions with random all-to-all interactions. These provide tractable models of the dynamics of quantum systems without quasiparticle excitations. The Kadanoff-Baym equations show that, at long times, the fermion two point function has a thermal form at a final temperature determined by energy conservation, and the numerical analysis is consistent with a thermalization rate proportional to this temperature. We also obtain an exact analytic solution of the quench dynamics in the large q limit of a model with q fermion interactions: in this limit, the thermalization of the two-point function is instantaneous.

I. INTRODUCTION

Investigating the dynamics of isolated quantum many-body systems is an essential question with wide-ranging implications to the fundamentals of statistical physics. The understanding of non-equilibrium quantum physics is important for a large variety of phenomena such as the dynamics of the early universe [1], heavy ion collisions at large hadron colliders [2], and pump and probe experiments [3] in condensed matter systems. Typically, the thermalization of quantum many body systems can be anticipated by recognizing ergodic behavior [4]. In contrast, a non-ergodic systems possess an extensive amount of local conserved quantities, which forbids thermalization. However, recent theoretical studies and experiments of strongly correlated systems advocate for a critical investigation of this naive categorization in ergodic and non-ergodic systems. For instance, the emergence of a time-scale leading to a quasistationary (or 'prethermal') state [5, 6], which still has fundamentally different properties from the true thermal equilibrium, goes already beyond the usual ergodic and non-ergodic behavior. Other examples, which go beyond this naive categorization, are one dimensional systems close to integrability, systems with slow modes preventing the thermalization of fast modes or interacting disordered systems.

The non-equilibrium dynamics of strongly interacting quantum many-particle systems are usually studied within the Schwinger-Keldysh formalism, which can describe evolution from a generic initial state to a final state which reaches thermal equilibrium at long times [7]. The thermodynamic parameters of the final state (*e.g.* temperature) are determined by the values of the conjugate conserved quantities (*e.g.* energy). The Kadanoff-Baym equations obtained from this formalism describe the manner and rate by which this final thermal state is reached.

The Kadanoff-Baym equations are usually too difficult to solve in their full generality. Frequently, a quasiparticle structure has been imposed on the spectral functions, so that the Kadanoff-Baym equations reduce to a quantum Boltzmann equation for the quasiparticle distribution functions. Clearly such an approach cannot be employed for final states of Hamiltonians which describe critical quantum matter *without* quasiparticle excitations. The most common approach is then to employ an expansion away from a regime where quasiparticles exist, using a small parameter such as the deviation of dimensionality from the critical dimension, or the inverse of the number of field components: the analysis is then

still carried out using quasiparticle distribution functions [8, 9].

In this paper, we will examine the non-equilibrium dynamics towards a final state without quasiparticles. We will *not* employ a quasiparticle decomposition, and instead provide solutions of the full Kadanoff-Baym equations. We can obtain non-equilibrium solutions for the Sachdev-Ye-Kitaev (SYK) models [10–12] with all-to-all and random interactions between q Majorana fermions on N sites. These models are solvable realizations of quantum matter without quasiparticles in equilibrium, and here we shall extend their study to non-equilibrium dynamics. We shall present numerical solutions of the Kadanoff-Baym equations for the fermion Green's function at $q = 4$, and an exact analytic solutions in the limit of large q (no quasiparticles are present in this limit). The large q solution relies on a remarkable exact SL(2,C) invariance, and has connections to quantum gravity on AdS_2 with the Schwarzian effective action [11–17] for the equilibrium dynamics, as we will note in Section V.

We find that the numerical $q = 4$ shows thermalization (of the two-point correlator) in a time of order the inverse final temperature: this thermalization rate is in accord with the fastest possible rate expected in non-quasiparticle systems [18]. In the large q limit, we find the surprising result that thermalization of the two-point correlator is instantaneous: the interpretation of this result is not fully clear from our results, but it could be an indication of a prethermal state appearing at $q = \infty$.

A. Model and results

The equilibrium SYK Hamiltonian we shall study is (using conventions from Ref. 12)

$$H = (i)^{\frac{q}{2}} \sum_{1 \leq i_1 < i_2 < \ldots < i_q \leq N} j_{i_1 i_2 \ldots i_q} \psi_{i_1} \psi_{i_2} \ldots \psi_{i_q} \tag{1.1}$$

where ψ_i are Majorana fermions on sites $i = 1 \ldots N$ obeying

$$\{\psi_i, \psi_j\} = \delta_{ij} \,, \tag{1.2}$$

and $j_{i_1 i_2 \ldots i_q}$ are independent Gaussian random variables with zero mean and variance

$$\langle j^2_{i_1 \ldots i_q} \rangle = \frac{J^2 (q-1)!}{N^{q-1}}. \tag{1.3}$$

These models are solvable realizations of quantum matter without quasiparticles. Here we shall study their non-equilibrium dynamics.

In the Schwinger-Keldysh formalism, observables are computed by evolving the initial state both forward and backwards along the closed time contour $\mathcal{C}$ [7], along which we define the contour-ordered Green's function

$$iG(t_1, t_2) = T_{\mathcal{C}} \langle \psi(t_1)\psi(t_2) \rangle \ . \tag{1.4}$$

The fields in the path integral are separated into components lying on the front and back of the contour. The two point functions of these fields define a matrix of Green's functions. Of these, we will be interested in the Majorana fermion greater(lesser) Green's functions $G^{>(<)}(t_1, t_2)$ defined as follows

$$G^{>}(t_1, t_2) \equiv G(t_1^-, t_2^+) \,, \tag{1.5a}$$

$$G^{<}(t_1, t_2) \equiv G(t_1^+, t_2^-) \tag{1.5b}$$

where t_i^- lives on the lower contour and t_i^+ on the upper contour.

Often one proceeds by doing a Keldysh rotation to express the Green's function in terms of its retarded, advanced, and Keldysh components. One can then use this information to study the evolution of the Keldysh Green's function. However, for Majorana fermions we have the condition

$$G^{>}(t_1, t_2) = -G^{<}(t_2, t_1). \tag{1.6}$$

This condition continues to hold even out of equilibrium [19]. This conveniently allows us to directly study a single component of the Green's function and then use Eq.(1.6) to construct all other Green's functions. The time evolution of the greater Green's function is governed by the Kadanoff-Baym equations derived from the non-equilibrium Dyson equation. We will study the non-equilibrium dynamics of the SYK model by solving the Kadanoff-Baym equations for the greater Green's function and tracking it's evolution after a quantum quench.

We start with a preliminary discussion of the closed time path integral formalism for Majorana fermions in Section II and compute the disorder averaged partition function for the SYK model with $q = 2$ and $q = 4$ interactions. We will then derive the Schwinger-Dyson equations on the closed time contour, and in turn use them to derive the Kadanoff-Baym equations on the real time axis. See also the related analysis of Ref. 20.

In Section III we will present numerical solutions of the Kadanoff-Baym equations for an SYK model with time-dependent $q = 2$ and $q = 4$ terms. Although several protocols are considered, the most interesting results appear for the following quench protocol. For

$t < 0$, we start with a thermal state with both $q = 2$ and $q = 4$ interactions present. In this case the $q = 2$ free fermion terms dominate at low energies, and hence we have Fermi liquid behavior at low temperatures. At $t = 0$ we switch off the $q = 2$ term so that we have only the $q = 4$ Hamiltonian as in Eq. (1.1) for $t > 0$. This Hamiltonian describes a non-Fermi liquid even at the lowest energies [10]. Just after the quench at $t = 0$, the system is in a non-equilibrium state. We show from the Kadanoff-Baym equations, and verify by our numerical analysis, that at late times the greater Green's function satisfies a Kubo-Martin-Schwinger (KMS) condition for a non-Fermi liquid state at $q = 4$ for an inverse temperature $\beta_f = 1/T_f$: this implies that the two-point correlator has the thermal equilibrium value at the inverse temperature β_f. The value of β_f is such that the total energy of the system remains the same after the quench at $t = 0^+$.

We will describe the time evolution of the system for $t \geq 0$ by computing a number of two-point fermion Green's functions $G(t_1, t_2)$. As the system approaches equilibrium, it is useful to characterize this correlator in terms of the absolute and relative times given by

$$\mathcal{T} = (t_1 + t_2)/2 \quad , \quad t = t_1 - t_2 \, . \tag{1.7}$$

For $\mathcal{T} \to \infty$ we have

$$\lim_{\mathcal{T} \to \infty} G(t_1, t_2) = G_{\beta_f}(t) \tag{1.8}$$

where G_{β_f} is the correlator in equilibrium at an inverse temperature β_f. For large $\mathcal{T}$ we will characterize $G(t_1, t_2)$ by an effective temperature $\beta_{\rm eff}(\mathcal{T})$. From our numerical analysis we characterize the late time approach to equilibrium by

$$\beta_{\rm eff}(\mathcal{T}) = \beta_f + \alpha \exp\left(-\Gamma \, \mathcal{T}\right) \, . \tag{1.9}$$

This defines a thermalization rate, Γ. Our complete numerical results for Γ appear in Fig. 3, and reasonably fit the behavior

$$\Gamma = C/\beta_f \quad , \quad \beta_f J_4 \gg 1 \, , \tag{1.10}$$

where C is a numerical constant independent of the initial state. Thus, at low final temperatures, the thermalization rate of the non-Fermi liquid two-point function appears proportional to temperature, as is expected for systems without quasiparticle excitations [18].

In Section IV we obtain exact analytic solutions of the Kadanoff-Baym equation in the limit of large q (no quasiparticles are present in this limit), where q refers to the number of fermions in the interaction in Eq. (1.1). This limit allows us to study corrections to the low temperature conformal solution and obtain equations that are exactly solvable. The large q solution relies on a remarkable exact SL(2,C) invariance, and has connections to quantum gravity on AdS_2 with the Schwarzian effective action [11–17]. For this limit, we will consider a model in which the $t < 0$ Hamiltonian has both a q-fermion interaction $\mathcal{J}$, and a pq fermion interaction $\mathcal{J}_p$. At $t > 0$, we quench to only a q fermion interaction $\mathcal{J}$. We will show that the non-equilibrium dynamics of this model are exactly solvable in the limit of large q taken at fixed p.

For $t_1 > 0$ or $t_2 > 0$ we find, in the large q limit of Section IV, that the $1/q$ correction to the Green's function (defined as in Eq. (4.1)), $g(t_1, t_2)$, obeys the two-dimensional Liouville equation. The most general solution of the Liouville equation can be written as [21]

$$g(t_1, t_2) = \ln \left[\frac{-h_1'(t_1) h_2'(t_2)}{\mathcal{J}^2 (h_1(t_1) - h_2(t_2))^2} \right] , \tag{1.11}$$

where $h_1(t_1)$ and $h_2(t_2)$ are arbitrary functions of their arguments. A remarkable and significant feature of this expression for $g(t_1, t_2)$ is that it is exactly invariant under SL(2,C) transformations of the functions $h_{1,2}(t)$. We will use the Schwinger-Keldysh analysis to derive ordinary differential equations that are obeyed by $h_{1,2}(t)$ in Section IV. Naturally, these equations will also be invariant under SL(2,C) transformations. We will show that for generic initial conditions in the regime $t_1 < 0$ and $t_2 < 0$, the solutions for $h_1(t_1)$ and $h_2(t_2)$ at $t_1 > 0$ and $t_2 > 0$ can be written in terms of four complex constants a, b, c, d, two real constants σ, θ are determined by the initial conditions in the $t_1 < 0$ and $t_2 < 0$ quadrant of the t_1-t_2 plane.

A surprising feature of our large q solutions is that for all $t_1 > 0$ and $t_2 > 0$ the result in Eq. (1.11) depends *only* upon the relative time t, and not on the average time $\mathcal{T}$. Further, we find that the two point function obeys a KMS condition [12, 22] at an inverse temperature determined by the two real constants σ and θ. This shows that the large q limit yields a solution in which the fermion two-point function thermalizes instantaneously at $t = 0^+$. This could indicate that the thermalization rate Γ diverges as at $q \to \infty$. Alternatively, as pointed out to us by Aavishkar Patel, the present large q solution could describe a pre-thermal state, and adding the $1/q^2$ corrections will give a finite thermalization rate; in such

a scenario, thermalization is a two-step process, with the first step occuring much faster than the second. However, we will not examine the $1/q^2$ corrections here to settle this issue.

II. KADANOFF-BAYM EQUATIONS FROM THE PATH INTEGRAL

We will consider the following time-dependent Hamiltonian

$$H(t) = i\sum_{i<j} j_{2,ij}\, f(t)\, \psi_i\psi_j - \sum_{i<j<k<l} j_{4,ijkl}\, g(t)\, \psi_i\psi_j\psi_k\psi_l, \tag{2.1}$$

where $j_{2,ij}$ and $j_{4,ijkl}$ are random variables as described in Eq. (1.3), and $f(t)$ and $g(t)$ are arbitrary functions of time. We will use $f(t)$ and $g(t)$ to specify the quench protocol by using them to turn on(off) or rescale couplings. We construct the path integral for this Hamiltonian of Majorana fermions from the familiar complex fermion path integral [23] by expressing the complex fermions Ψ_i in terms of two real fermions ψ_i and χ_i i.e. $\Psi_i = \psi_i + i\chi_i$. Since χ_i is just a spectator which does not appear in the Hamiltonian, we can disregard its contribution and write the path integral representation of the partition function as

$$Z = \int D\psi \int Dj_{2,ij} \int Dj_{4,ijkl} P(j_{4,ijkl}) P(j_{2,ij}) e^{iS[\psi]}\,, \tag{2.2}$$

with the action

$$S[\psi] = \int_{\mathcal{C}} dt \Big\{ \frac{i}{2}\sum_i \psi_i\partial_t\psi_i - i\sum_{i<j} j_{2,ij} f(t)\psi_i\psi_j + \sum_{i<j<k<l} j_{4,ijkl} g(t)\psi_i\psi_j\psi_k\psi_l \Big\}. \tag{2.3}$$

Here, the Majorana fields ψ_i live on the closed time contour $\mathcal{C}$, and Z is normalized to one. The probability distributions of $j_{2,ij}$ and $j_{4,ijkl}$ are given by

$$\mathcal{P}_1(j_{2,ij}) = \sqrt{\frac{N}{2J_2^2\pi}} \exp\Big(-\frac{N}{2J_2^2}\sum_{i<j} j_{2,ij}^2 \Big), \tag{2.4}$$

$$\mathcal{P}_2(j_{4,ijkl}) = \sqrt{\frac{N^3}{12J_4^2\pi}} \exp\Big(-\frac{N^3}{12J_4^2}\sum_{i<j<k<l} j_{4,ijkl}^2 \Big). \tag{2.5}$$

The normalization of Z allows us to directly average over disorder by performing the $j_{2,ij}$ and $j_{4,ijkl}$ integrals. This gives us the following path integral

$$Z = \int D\psi \exp\Big\{ -\frac{1}{2}\int_{\mathcal{C}} dt_1 \sum_i \psi_i\partial_{t_1}\psi_i - \frac{J_2^2}{4N}\sum_{i,j}\int_{\mathcal{C}} dt_1 \int_{\mathcal{C}} dt_2 f(t_1)f(t_2)\psi_i(t_1)\psi_i(t_2)\psi_j(t_1)\psi_j(t_2) \\ - \frac{3J_4^2}{4!N^3}\sum_{i,j,k,l}\int_{\mathcal{C}} dt_1 \int_{\mathcal{C}} dt_2 g(t_1)g(t_2)\psi_i(t_1)\psi_i(t_2)\psi_j(t_1)\psi_j(t_2)\psi_k(t_1)\psi_k(t_2)\psi_l(t_1)\psi_l(t_2) \Big\}\,,$$

where the action is bi-local in time. We introduce the bi-linear field G (the Green's function)

$$G(t_1, t_2) = -\frac{i}{N}\sum_i \psi_i(t_1)\psi_i(t_2)\,. \tag{2.6}$$

and impose Eq. (2.6) by a Lagrange multiplier Σ (which will turn out to be the self energy). This leads to the following partition function

$$Z = \int D\psi \int DG \int D\Sigma \exp\Big\{-\frac{1}{2}\int_{\mathcal{C}} dt_1 \sum_i \psi_i \partial_{t_1}\psi_i + \frac{J_2^2 N}{4}\int_{\mathcal{C}} dt_1 \int_{\mathcal{C}} dt_2 f(t_1)f(t_2)G(t_1,t_2)^2$$
$$- \frac{3J_4^2 N}{4!}\int_{\mathcal{C}} dt_1 \int_{\mathcal{C}} dt_2 g(t_1)g(t_2)G(t_1,t_2)^4 + \frac{i}{2}\int_{\mathcal{C}} dt_1 \int_{\mathcal{C}} dt_1 \Sigma(t_1,t_2)\big[G(t_1,t_2) + \frac{i}{N}\sum_i \psi_i(t_1)\psi_i(t_2)\big]\Big\}.$$

Rescaling integration variables as $\Sigma \to iN\Sigma$ and integrating out the fermion yields

$$Z = \int DG \int D\Sigma \exp\Big\{iS\big[G,\Sigma\big]\Big\}\,, \tag{2.7}$$

with the action written in terms of G and Σ

$$\begin{aligned} S\big[G,\Sigma\big] = &-\frac{iN}{2}\,\mathrm{tr}\log\big[-i(G_0^{-1}-\Sigma)\big] - \frac{iJ_2^2 N}{4}\int_{\mathcal{C}} dt_1 \int_{\mathcal{C}} dt_2 f(t_1)f(t_2)G(t_1,t_2)^2 \\ &+ \frac{3iJ_4^2 N}{4!}\int_{\mathcal{C}} dt_1 \int_{\mathcal{C}} dt_2 g(t_1)g(t_2)G(t_1,t_2)^4 + \frac{iN}{2}\int_{\mathcal{C}} dt_1 \int_{\mathcal{C}} dt_2 \Sigma(t_1,t_2)G(t_1,t_2) \end{aligned} \tag{2.8}$$

where G_0 is the free Majorana Green's function and $G_0^{-1}(t_1,t_2) = i\partial_t \delta_{\mathcal{C}}(t_1,t_2)$. Varying the action with respect to Σ and G yields the Schwinger-Dyson equations for the Green's function and self-energy:

$$G_0^{-1}(t_1,t_2) - G^{-1}(t_1,t_2) = \Sigma(t_1,t_2)\,, \tag{2.9}$$

$$\Sigma(t_1,t_2) = J_2^2 f(t_1)f(t_2)G(t_1,t_2) - J_4^2 g(t_1)g(t_2)G(t_1,t_2)^3. \tag{2.10}$$

Note that the time arguments are with respect to the closed time contour making the matrix structure of the full Green's function implicit. The bare greater and lesser Green's functions for the Majorana fermions are given by

$$G_0^{>}(t_1,t_2) = -\frac{i}{2}\,. \tag{2.11}$$

We now use $G^>$ and $G^<$ to define the retarded, advanced and Keldysh Green's functions:

$$G^R(t_1,t_2) \equiv \Theta(t_1-t_2)\big[G^>(t_1,t_2) - G^<(t_1,t_2)\big]\,, \tag{2.12a}$$

$$G^A(t_1,t_2) \equiv \Theta(t_2-t_1)\big[G^<(t_1,t_2) - G^>(t_1,t_2)\big]\,, \tag{2.12b}$$

$$G^K(t_1,t_2) \equiv G^>(t_1,t_2) + G^<(t_1,t_2)\,. \tag{2.12c}$$

Similarly, we introduce retarded and advanced self-energies

$$\Sigma^R(t_1,t_2) \equiv \Theta(t_1-t_2)\left[\Sigma^>(t_1,t_2)-\Sigma^<(t_1,t_2)\right], \tag{2.13}$$

$$\Sigma^A(t_1,t_2) \equiv -\Theta(t_2-t_1)\left[\Sigma^>(t_1,t_2)-\Sigma^<(t_1,t_2)\right] \tag{2.14}$$

For more details on the Schwinger-Keldysh formalism and the saddle point approximation we refer to Refs. 7, 12, and 19.

To obtain the Kadanoff-Baym equations, we rewrite the Schwinger-Dyson equations in (2.9) as

$$\int_{\mathcal{C}} dt_3 G_0^{-1}(t_1,t_3)G(t_3,t_2) = \delta_{\mathcal{C}}(t_1,t_2) + \int_{\mathcal{C}} dt_3 \Sigma(t_1,t_3)G(t_3,t_2)\,, \tag{2.15}$$

$$\int_{\mathcal{C}} dt_3 G(t_1,t_3)G_0^{-1}(t_3,t_2) = \delta_{\mathcal{C}}(t_1,t_2) + \int_{\mathcal{C}} dt_3 G(t_1,t_3)\Sigma(t_3,t_2)\,. \tag{2.16}$$

Using the Langreth rules described in Ref. 24, we rewrite Eq. (2.15) and Eq. (2.16) on the real time axis as

$$\int_{\mathcal{C}} dt_3 \Sigma(t_1^+,t_3)G(t_3,t_2^+) = \int_{-\infty}^{\infty} dt_3 \left\{\Sigma^R(t_1,t_3)G^>(t_3,t_2)+\Sigma^>(t_1,t_2)G^A(t_2,t_3)\right\}, \tag{2.17}$$

$$\int_{\mathcal{C}} dt_3 G(t_1^+,t_3)\Sigma(t_3,t_2^+) = \int_{-\infty}^{\infty} dt_3 \left\{G^R(t_1,t_3)\Sigma^>(t_3,t_2)+G^>(t_1,t_2)\Sigma^A(t_2,t_3)\right\}, \tag{2.18}$$

The last equation gives us the following equations of motion for $G^>$

$$i\partial_{t_1} G^>(t_1,t_2) = \int_{-\infty}^{\infty} dt_3 \Big\{\Sigma^R(t_1,t_3)G^>(t_3,t_2)+\Sigma^>(t_1,t_3)G^A(t_3,t_2)\Big\}, \tag{2.19}$$

$$-i\partial_{t_2} G^>(t_1,t_2) = \int_{-\infty}^{\infty} dt_3 \Big\{G^R(t_1,t_3)\Sigma^>(t_3,t_2)+G^>(t_1,t_3)\Sigma^A(t_3,t_2)\Big\}, \tag{2.20}$$

where

$$\Sigma^>(t_1,t_2) = J_2^2 f(t_1)f(t_2)G^>(t_1,t_2) - J_4^2 g(t_1)g(t_2)\big(G^>(t_1,t_2)\big)^3 \tag{2.21}$$

and Σ^R and Σ^A are defined in Eq. (2.13) and Eq. (2.14). In Section III, we will solve this system of equations numerically. Analytic solutions for the generalization of this model in the large q limit will appear in Section IV.

III. KADANOFF-BAYM EQUATIONS: NUMERICAL STUDY

All of the quench protocols we considered are of the form

$$f(t) = \alpha_1\Theta(-t)+\alpha_2\Theta(t)\,,$$
$$g(t) = \gamma_1\Theta(-t)+\gamma_2\Theta(t)\,, \tag{3.1}$$

where $\Theta(t)$ is the unit step function, and will be denoted by $(J_{2,i}, J_{4,i}) \to (J_{2,f}, J_{4,f})$. Specifically, we choose the following four protocols

A) $(J_{2,i}, 0) \to (J_{2,f}, 0)$ quench: the energy scale of the random hopping model gets suddenly rescaled.

B) $(0, 0) \to (0, J_{4,f})$ quench: the system is quenched from an uncorrelated state by switching on the interaction of the SYK model.

C) $(J_{2,i}, 0) \to (0, J_{4,f})$ quench: the system is prepared in the ground state of the random hopping model and then quenched to the SYK Hamiltonian.

D) $(J_{2,i}, J_{4,f}) \to (0, J_4)$ quench: starting from a ground state with the quadratic and the quartic terms present the quadratic term is switched off.

The numerical results for quenches A-C appear in Appendix D, while those for the most interesting case of quench D appear below.

The Kadanoff-Baym equations for the SYK model (Eqs. (2.19) and (2.20)) are solved numerically for each quench protocol described above. The absence of momentum dependence will allow us to explore dynamics at long times after the quench. We set the quench time to $t_1 = t_2 = 0$. For $t_1 < 0$ and $t_2 < 0$, we are in thermal equilibrium and the time dependence of the Green's function is determined by the Dyson equation. When quenching the ground state of the random hopping model, we can use the exact solution for $G^>$ as an initial condition. In all other cases, we solve the Dyson equation self-consistently: for further details we refer to Appendix C. Using the boundary conditions given by pre-quench state, we solve Kadanoff-Baym equation for $t_1 > 0$ or $t_2 > 0$, and obtain the post-quench evolution of $G^>$. Integrals in the Kadanoff-Baym equation are computed using the trapezoidal rule. After discretizing the integrals, the remaining ordinary differential equations are solved using a predictor-corrector scheme, where the corrector is determined self-consistently by iteration. For long times after the quench, the numerical effort is equivalent to a second-order Runge-Kutta scheme, because the self-consistency of the predictor-corrector scheme converges very fast. Using this approach right after the quench reduces numerical errors significantly.

To interpret the long time behavior Green's functions, we briefly comment on properties of thermal Green's functions. In thermal equilibrium, all Green's function only depend on

the relatice time t. The imaginary part of the Fourier transformed retarded Green's function is given by the spectral function

$$A(\omega) = -2\,\mathrm{Im}\,G^R(\omega)\,. \tag{3.2}$$

In thermal equilibrium, the Kubo-Martin-Schwinger (KMS) condition [7] establishes a relationship between $G^>(\omega)$ and $G^<(\omega)$ which is given by

$$G^>(\omega) = -e^{\beta\omega}G^<(\omega)\,. \tag{3.3}$$

Using the definition of G^R, we can write the spectral function in terms of $G^>$ as

$$A(\omega) = G^>(\omega)(1 + e^{-\beta\omega}). \tag{3.4}$$

Similarly the Keldysh component of the fermionic Green's function is related to the spectral function by

$$iG^K(\omega) = iG^>(\omega) + iG^<(\omega) = \tanh\big(\beta\omega/2\big)A(\omega)\,. \tag{3.5}$$

Out of equilibrium, the Green's we have defined functions depend on both τ and $\mathcal{T}$. However, we can still consider the Fourier transform with respect to t given by

$$G^R(\mathcal{T},\omega) = \int_0^\infty dt\, e^{-\delta t}e^{i\omega t}G^R(\mathcal{T}+t/2,\mathcal{T}-t/2)\,, \tag{3.6}$$

known as the Wigner transform. Using Eq. (3.6), we the express the spectral function out of equilibrium in terms of $\mathcal{T}$ and ω as

$$A(\mathcal{T},\omega) = -2\,\mathrm{Im}\,G^R(\mathcal{T},\omega). \tag{3.7}$$

We can compute the spectral function and the Keldysh component of the Green's function by numerically solving for $G^>(t_1,t_2)$. To investigate thermalization behaviour, at each $\mathcal{T}$

$$\text{we fit } \frac{iG^K(\mathcal{T},\omega)}{A(\mathcal{T},\omega)} \text{ to } \tanh\Big(\frac{\beta_{\text{eff}}(\mathcal{T})\omega}{2}\Big) \text{ at low } \omega. \tag{3.8}$$

and so determined a time-independent effective inverse temperature $\beta_{\text{eff}}(\mathcal{T})$. By Eq. (3.5), $\beta_{\text{eff}}(\mathcal{T})$ is the actual inverse temperature, β_f, in a thermal state reached as $\mathcal{T}\to\infty$.

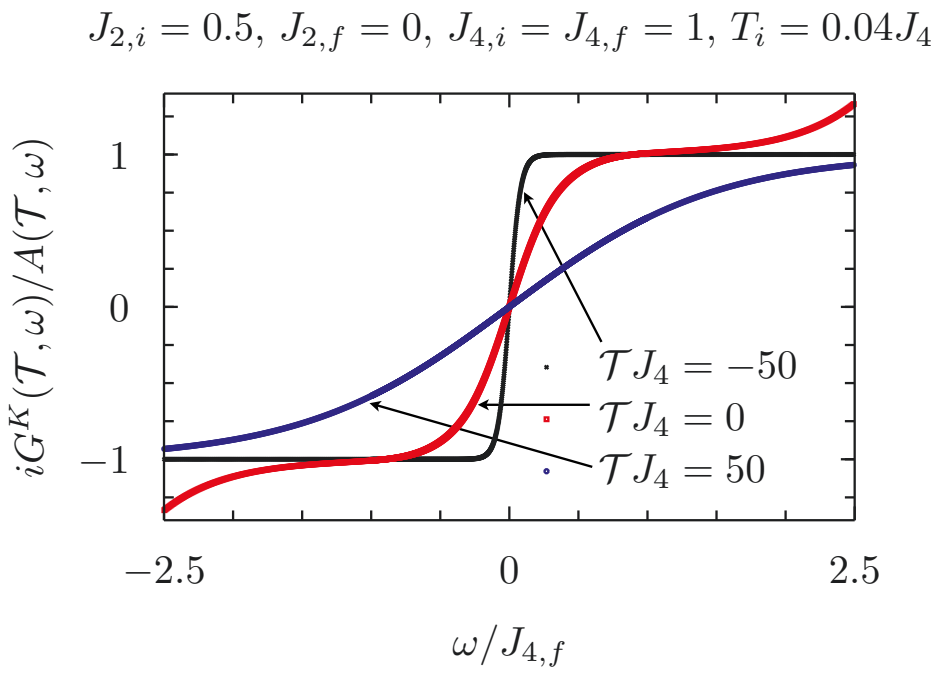

FIG. 1. The ratio of the Keldysh and spectral function is shown before and after a quench from a J_2+J_4 model to a purely J_4 model. Fits to this data allow determination of the effective temperature as a function of time after the quench, $\beta_{\rm eff}(\mathcal{T})$ using Eq. (3.8).

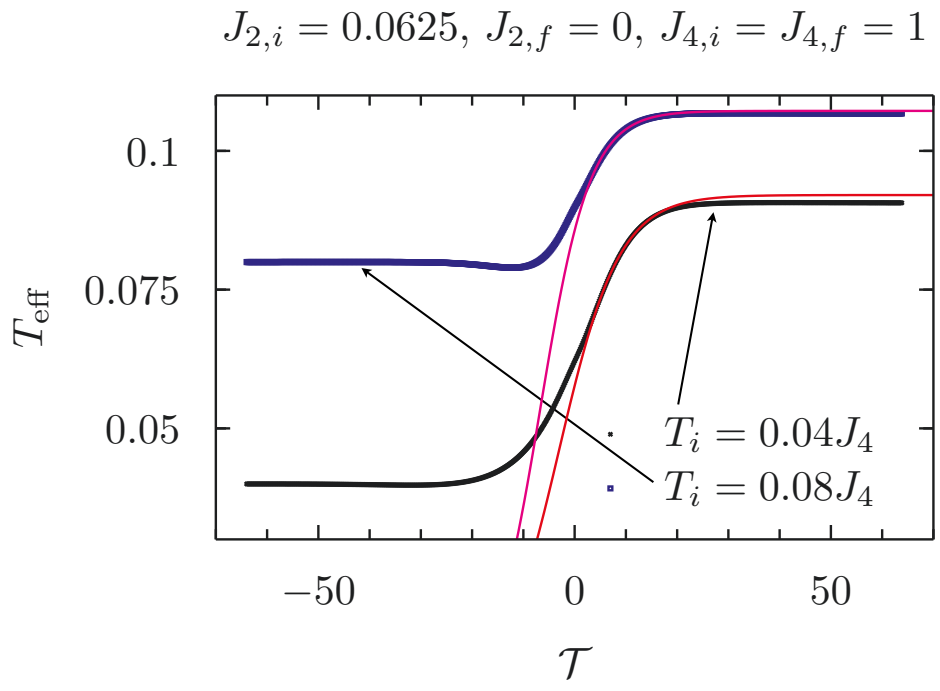

FIG. 2. Fits to the values of the effective temperature $\beta_{\rm eff}(\mathcal{T}) = 1/T_{\rm eff}(\mathcal{T})$ from results as in Fig. 1 to Eq. (1.9) to allow determination of the thermalization rate Γ for each quench.

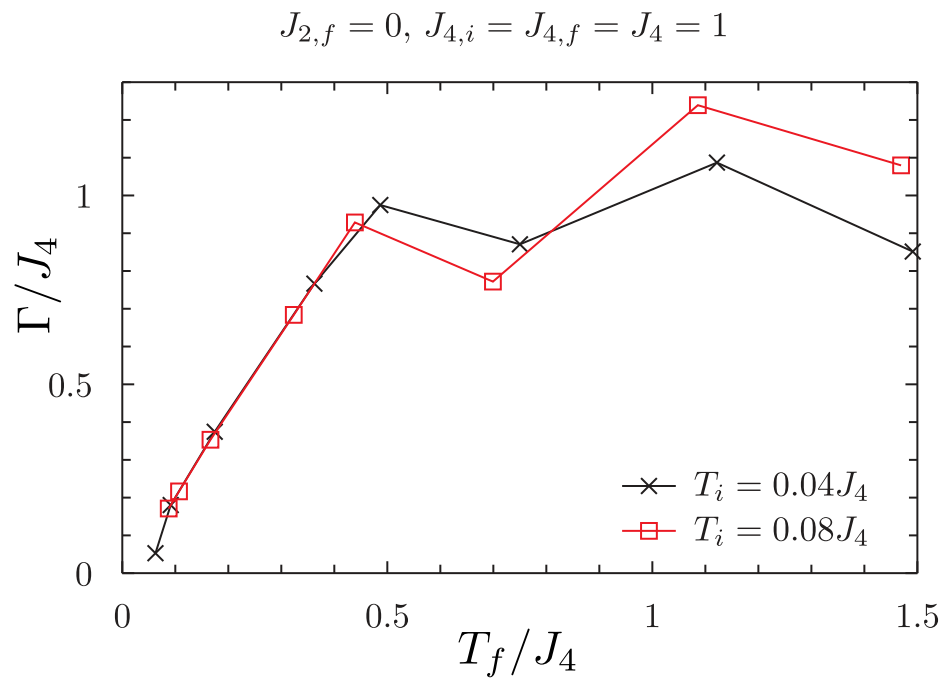

FIG. 3. The values of the thermalization rate Γ obtained from Fig. 2 are shown as a function of the final temperature, T_f, for each quench. One of our main numerical results is the proportionality of Γ to T_f at small $T_f \ll J$. At larger T_f, Γ is of order J_4.

A. Numerical results

We describe the results for quench D above, in which $(J_{2,i}, J_{4,i}) \to (0, J_{4,f})$ *i. e.* quenches from a Hamiltonian with a quadratic and a quartic term to a Hamiltonian where the quadratic term has been switched off. This quench results in nontrivial dynamics of the two-point function. To study thermalization, we can check the validity of the fluctuation-dissipation relation and the behavior of the effective temperature $T_{\rm eff}(\mathcal{T}) = \beta_{\rm eff}^{-1}(\mathcal{T})$ at times after the quench. The effective temperature can either be obtained from the derivative of $iG^K(\mathcal{T},\omega)/A(\mathcal{T},\omega)$ at $\omega = 0$, or as a fit of $\tanh[\omega/(2T_{\rm eff})]$ to that function to some frequency interval. As shown in Fig. 1, long after the quench, the numerical results for $iG^K(\mathcal{T},\omega)/A(\mathcal{T},\omega)$ are well described by $\tanh[\omega/(2T_{\rm eff})]$, indicating that the Green's function has thermalized. At intermediate times, the low frequency behaviour is still well described by this function. At high frequencies, deviations are visible, which indicate that $iG^K(\mathcal{T},\omega)/A(\mathcal{T},\omega)$ is non-thermal at such times.

Long after after the quench, the value of $T_{\rm eff}(\mathcal{T})$ relaxes exponentially rapidly to T_f.

In Fig. 2 we show the time-dependence of the effective temperature, and a fit of $T_{\rm eff}^{-1}$ to Eq. (1.9). The thermalization rate, Γ obtained from such fits is shown in Fig. 3. This rate appears proportional to the final temperature T_f at small final temperatures as noted in Eq. (1.10), and saturates at higher temperatures. It is difficult to determine Γ numerically at large T_f/J_4, and this likely leads to the oscillatory behavior present in Fig. 3.

IV. KADANOFF-BAYM EQUATIONS: LARGE q LIMIT

We will consider a model with a q fermion coupling $J(t)$, and a pq fermion coupling $J_p(t)$. For now, we keep the time-dependence of both couplings arbitrary. In the large q limit, the Green's function can be written as [12]

$$G^>(t_1,t_2) = -i\,\langle\psi(t_1)\psi(t_2)\rangle = -\frac{i}{2}\left[1+\frac{1}{q}g(t_1,t_2)+\ldots\right] \tag{4.1}$$

where

$$g(t,t) = 0\,. \tag{4.2}$$

A. Set-up

The Kadanoff-Baym equations in Eqs. (2.19), (2.20) and (2.21) for $G^>(t_1,t_2)$ now become

$$\begin{aligned}
i\frac{\partial}{\partial t_1}G^>(t_1,t_2) &= -i^q\int_{-\infty}^{t_1} dt_3\, J(t_1)J(t_3)\left[(G^>)^{q-1}(t_1,t_3)-(G^<)^{q-1}(t_1,t_3)\right]G^>(t_3,t_2)\\
&\quad + i^q\int_{-\infty}^{t_2} dt_3\, J(t_1)J(t_3)(G^>)^{q-1}(t_1,t_3)\left[G^>(t_3,t_2)-G^<(t_3,t_2)\right]\\
&\quad - i^{pq}\int_{-\infty}^{t_1} dt_3\, J_p(t_1)J_p(t_3)\left[(G^>)^{pq-1}(t_1,t_3)-(G^<)^{pq-1}(t_1,t_3)\right]G^>(t_3,t_2)\\
&\quad + i^{pq}\int_{-\infty}^{t_2} dt_3\, J_p(t_1)J_p(t_3)(G^>)^{pq-1}(t_1,t_3)\left[G^>(t_3,t_2)-G^<(t_3,t_2)\right]\,,\\
-i\frac{\partial}{\partial t_2}G^>(t_1,t_2) &= -i^q\int_{-\infty}^{t_1} dt_3\, J(t_3)J(t_2)\left[G^>(t_1,t_3)-G^<(t_1,t_3)\right](G^>)^{q-1}(t_3,t_2)\\
&\quad + i^q\int_{-\infty}^{t_2} dt_3\, J(t_3)J(t_2)G^>(t_1,t_3)\left[(G^>)^{q-1}(t_3,t_2)-(G^<)^{q-1}(t_3,t_2)\right]\\
&\quad - i^{pq}\int_{-\infty}^{t_1} dt_3\, J_p(t_3)J_p(t_2)\left[G^>(t_1,t_3)-G^<(t_1,t_3)\right](G^>)^{pq-1}(t_3,t_2)\\
&\quad + i^{pq}\int_{-\infty}^{t_2} dt_3\, J_p(t_3)J_p(t_2)G^>(t_1,t_3)\left[(G^>)^{pq-1}(t_3,t_2)-(G^<)^{pq-1}(t_3,t_2)\right]\,.
\end{aligned} \tag{4.3}$$

where we have defined

$$J_p(t) \equiv J_p f(t) \quad , \quad J(t) \equiv J g(t) \, . \tag{4.4}$$

Also, recall that Eq. (1.6) relates $G^>$ to $G^<$.

We note a property of the Kadanoff-Baym equations in Eq. (4.3), connected to a comment in Section I above Eq. (1.7). If we set $J_p(t) = 0$, then all dependence of Eq. (4.3) on $J(t)$ can be scaled away by reparameterizing time via

$$\int^t J(t')dt' \to t \, . \tag{4.5}$$

This implies that correlation functions remain in thermal equilibrium in the new time coordinate. However, when both $J_p(t)$ and $J(t)$ are non-zero, such a reparameterization is not sufficient, and there are non-trivial quench dynamics, as shown in our numerical study in Section III. Below, we will see that the quench dynamics can also be trivial in the limit $q \to \infty$, even when both $J_p(t)$ and $J(t)$ are both non-zero. This result arises from fairly non-trivial computations which are described below, and in particular from an SL(2,C) symmetry of the parameterization of the equations.

In the large q limit, we assume a solution of the form in Eq. (4.1). Inserting Eq. (4.1) into Eq. (4.3), we obtain to leading order in $1/q$

$$\begin{aligned}
\frac{\partial}{\partial t_1} g(t_1,t_2) &= 2\int_{-\infty}^{t_2} dt_3 \, \mathcal{J}(t_1)\mathcal{J}(t_3) e^{g(t_1,t_3)} - \int_{-\infty}^{t_1} dt_3 \, \mathcal{J}(t_1)\mathcal{J}(t_3)\left[e^{g(t_1,t_3)} + e^{g(t_3,t_1)}\right] \\
&+ 2\int_{-\infty}^{t_2} dt_3 \, \mathcal{J}_p(t_1)\mathcal{J}_p(t_3) e^{pg(t_1,t_3)} - \int_{-\infty}^{t_1} dt_3 \, \mathcal{J}_p(t_1)\mathcal{J}_p(t_3)\left[e^{pg(t_1,t_3)} + e^{pg(t_3,t_1)}\right] \, , \\
\frac{\partial}{\partial t_2} g(t_1,t_2) &= 2\int_{-\infty}^{t_1} dt_3 \, \mathcal{J}(t_3)\mathcal{J}(t_2) e^{g(t_3,t_2)} - \int_{-\infty}^{t_2} dt_3 \, \mathcal{J}(t_3)\mathcal{J}(t_2)\left[e^{g(t_3,t_2)} + e^{g(t_2,t_3)}\right] \\
&+ 2\int_{-\infty}^{t_1} dt_3 \, \mathcal{J}_p(t_3)\mathcal{J}_p(t_2) e^{pg(t_3,t_2)} - \int_{-\infty}^{t_2} dt_3 \, \mathcal{J}_p(t_3)\mathcal{J}_p(t_2)\left[e^{pg(t_3,t_2)} + e^{pg(t_2,t_3)}\right] \, ,
\end{aligned} \tag{4.6}$$

where

$$\mathcal{J}^2(t) = qJ^2(t)2^{1-q} \quad , \quad \mathcal{J}_p^2(t) = qJ_p^2(t)2^{1-pq} \tag{4.7}$$

Remarkably, these non-linear, partial, integro-differential equations are exactly solvable for our quench protocol and all other initial conditions, as we will show in the remainder of this section. The final exact solution appears in Section IV E, and surprisingly shows that the solution is instantaneously in thermal equilibrium at $t = 0^+$.

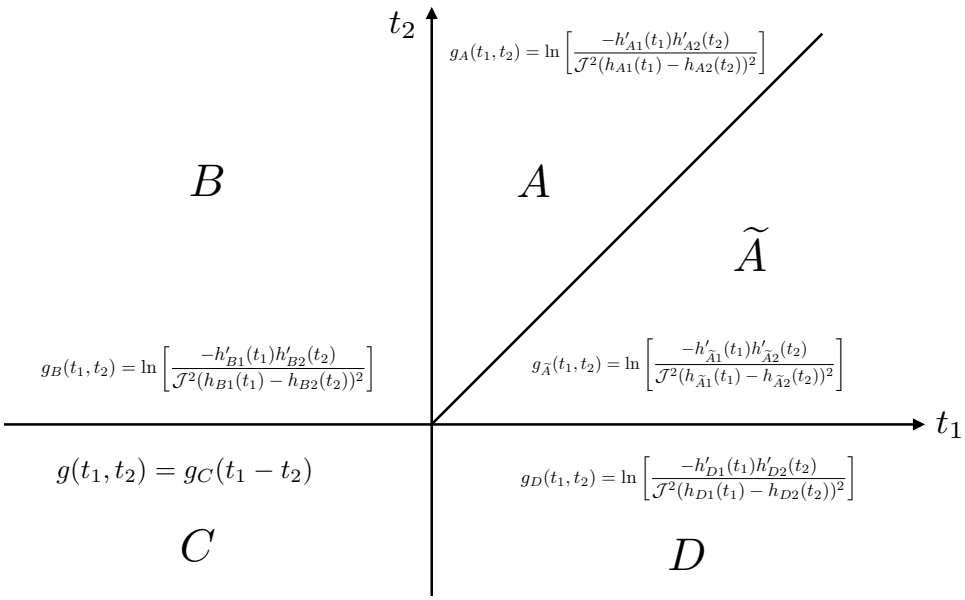

FIG. 4. The regions in the t_1-t_2 plane.

The key to the exact solution is to take derivatives of either equation in Eq. (4.6) to obtain

$$\frac{\partial^2}{\partial t_1 \partial t_2} g(t_1,t_2) = 2\mathcal{J}(t_1)\mathcal{J}(t_2)e^{g(t_1,t_2)} + 2\mathcal{J}_p(t_1)\mathcal{J}_p(t_2)e^{pg(t_1,t_2)}\,. \tag{4.8}$$

We will look at the case where $\mathcal{J}_p(t)$ is non-zero only for $t<0$, while $\mathcal{J}(t)$ is time independent:

$$\mathcal{J}_p(t) = \mathcal{J}_p\,\Theta(-t) \quad , \quad \mathcal{J}(t) = \mathcal{J}\,; \tag{4.9}$$

This is the analog of the protocol D in Section III. In this case, Eq. (4.8) is the Lorentzian Liouville equation

$$\frac{\partial^2}{\partial t_1 \partial t_2} g(t_1,t_2) = 2\mathcal{J}^2\, e^{g(t_1,t_2)}\,, \tag{4.10}$$

in three of the four quadrants of the t_1-t_2 plane (labeled as in Fig. 4). The most general solution of Eq. (4.10) in these quadrants is

$$g_\alpha(t_1,t_2) = \ln\left[\frac{-h'_{\alpha1}(t_1)h'_{\alpha2}(t_2)}{\mathcal{J}^2(h_{\alpha1}(t_1)-h_{\alpha2}(t_2))^2}\right] \quad , \quad \text{for } \alpha = A,\widetilde{A},B,D\,. \tag{4.11}$$

Eq. (4.11) will also apply for $\alpha = C$ when $\mathcal{J}_p = 0$. Eq. (4.2) implies that the functions $h_{A1}(t)$ and $h_{A2}(t)$ obey

$$h'_{A1}(t)h'_{A2}(t) = -\mathcal{J}^2(h_{A1}(t)-h_{A2}(t))^2\,, \tag{4.12}$$

and similarly

$$h'_{\widetilde{A}1}(t)h'_{\widetilde{A}2}(t) = -\mathcal{J}^2(h_{\widetilde{A}1}(t) - h_{\widetilde{A}2}(t))^2\,, \tag{4.13}$$

A crucial feature of Eq. (4.11) is that $g_\alpha(t_1, t_2)$ remains invariant under the SL(2,C) transformation which maps both $h_{\alpha 1}$ and $h_{\alpha 2}$ by the same transformation

$$h(t) \to \frac{a\,h(t) + b}{c\,h(t) + d}\,, \tag{4.14}$$

where a, b, c, d are complex numbers obeying $ad - bc = 1$. This transformation can be differ in different regions, α, of the t_1,t_2 plane.

Given the symmetries of Eq. (4.6) and the thermal initial conditions, we look for solutions which obey

$$g(t_2, t_1) = [g(t_1, t_2)]^*\,. \tag{4.15}$$

This property can be related to the causality of the Kadanoff-Baym equations as is explained in Appendix E. We can satisfy Eq. (4.15) in quadrants A, B, D by the relations

$$\begin{aligned} h_{\widetilde{A}1}(t) &= h^*_{A2}(t)\,, \\ h_{\widetilde{A}2}(t) &= h^*_{A1}(t)\,, \\ h_{D1}(t) &= h^*_{B2}(t)\,, \\ h_{D2}(t) &= h^*_{B1}(t)\,. \end{aligned} \tag{4.16}$$

The solution in Eq. (4.11) applies in all but the C quadrant of Fig. 4. In quadrant C, the system is in thermal equilibrium, and so the Green's function depends only upon time differences. We describe this equilibrium solution in Appendix F. In the following subsections, we describe the results of inserting the parameterization in Eq. (4.11) back into Eq. (4.6) to obtain ordinary differential equations for $h_{\alpha 1}$ and $h_{\alpha 2}$ in the remainder of the t_1-t_2 plane.

B. Quadrant B

From Eq. (4.6), we obtain for $t_1 < 0$ and $t_2 > 0$

$$-\frac{\partial}{\partial t_1} g_B(t_1,t_2) = -\mathcal{J}^2 \int_{-\infty}^{\infty} dt'\, e^{g_C(t')}\, \mathrm{sgn}(t'-t_1) - 2\mathcal{J}^2 \int_0^{t_2} dt_3\, e^{g_B(t_1,t_3)} - \mathcal{J}_p^2 \int_{-\infty}^{\infty} dt' \mathrm{sgn}(t'-t_1) e^{p g_C(t')}\,,$$

$$\frac{\partial}{\partial t_2} g_B(t_1,t_2) = 2\mathcal{J}^2 \int_{-\infty}^{t_1} dt_3\, e^{g_B(t_3,t_2)} - \mathcal{J}^2 \int_{-\infty}^{0} dt_3\, \left[e^{g_B(t_3,t_2)} + e^{g_D(t_2,t_3)}\right] - \mathcal{J}^2 \int_0^{t_2} dt_3\, \left[e^{g_A(t_3,t_2)} + e^{g_{\tilde{A}}(t_2,t_3)}\right]\,. \tag{4.17}$$

Inserting Eq. (4.11) in Eq. (4.17) we obtain

$$-\frac{h''_{B1}(t_1)}{h'_{B1}(t_1)} = -\mathcal{J}^2 \int_{-\infty}^{\infty} dt'\, e^{g_C(t')}\, \mathrm{sgn}(t'-t_1) - \frac{2h'_{B1}(t_1)}{h_{B1}(t_1) - h_{B2}(0)} - \mathcal{J}_p^2 \int_{-\infty}^{\infty} dt' \mathrm{sgn}(t'-t_1) e^{p g_C(t')}\,, \tag{4.18}$$

$$\frac{h''_{B2}(t_2)}{h'_{B2}(t_2)} = -\frac{2h'_{B2}(t_2)}{h_{B1}(-\infty) - h_{B2}(t_2)} - \frac{h'_{B2}(t_2)}{h_{B1}(0) - h_{B2}(t_2)} + \frac{h'_{B2}(t_2)}{h_{B1}(-\infty) - h_{B2}(t_2)} - \frac{h^{*\prime}_{B2}(t_2)}{h^*_{B1}(0) - h^*_{B2}(t_2)} + \frac{h^{*\prime}_{B2}(t_2)}{h^*_{B1}(-\infty) - h^*_{B2}(t_2)} - \frac{h'_{A2}(t_2)}{h_{A1}(t_2) - h_{A2}(t_2)} + \frac{h'_{A2}(t_2)}{h_{A1}(0) - h_{A2}(t_2)} - \frac{h^{*\prime}_{A2}(t_2)}{h^*_{A1}(t_2) - h^*_{A2}(t_2)} + \frac{h^{*\prime}_{A2}(t_2)}{h^*_{A1}(0) - h^*_{A2}(t_2)}\,. \tag{4.19}$$

We also have the compatibility condition at the boundary between regions B and C, which is

$$g_C(t_1) = \ln\left[\frac{-h'_{B1}(t_1) h'_{B2}(0)}{\mathcal{J}^2 (h_{B1}(t_1) - h_{B2}(0))^2}\right]\,; \tag{4.20}$$

taking the derivative of this equation we obtain precisely the first equation in Eq. (4.18) after using Eq. (F2). This reassures us that the system of equations are not overdetermined. We can easily integrate Eq. (4.20) to obtain

$$\frac{h'_{B2}(0)}{h_{B1}(t_1) - h_{B2}(0)} - \frac{h'_{B2}(0)}{h_{B1}(-\infty) - h_{B2}(0)} = \mathcal{J}^2 \int_{-\infty}^{t_1} dt\, e^{g_C(t)}\,. \tag{4.21}$$

C. Region A

Now $t_2 > t_1 > 0$. From the second Eq. (4.6) we obtain

$$\frac{\partial}{\partial t_2} g_A(t_1,t_2) = 2\mathcal{J}^2 \int_{-\infty}^{0} dt_3\, e^{g_B(t_3,t_2)} + 2\mathcal{J}^2 \int_0^{t_1} dt_3\, e^{g_A(t_3,t_2)} - \mathcal{J}^2 \int_{-\infty}^{0} dt_3\, \left[e^{g_B(t_3,t_2)} + e^{g_D(t_2,t_3)}\right] - \mathcal{J}^2 \int_0^{t_2} dt_3\, \left[e^{g_A(t_3,t_2)} + e^{g_{\tilde{A}}(t_2,t_3)}\right]\,. \tag{4.22}$$

Inserting Eq. (4.11) into Eq. (4.22), we obtain

$$\begin{aligned}\frac{h''_{A2}(t_2)}{h'_{A2}(t_2)} = &\frac{2h'_{B2}(t_2)}{h_{B1}(0)-h_{B2}(t_2)} - \frac{2h'_{B2}(t_2)}{h_{B1}(-\infty)-h_{B2}(t_2)} - \frac{2h'_{A2}(t_2)}{h_{A1}(0)-h_{A2}(t_2)} \\ &- \frac{h'_{B2}(t_2)}{h_{B1}(0)-h_{B2}(t_2)} + \frac{h'_{B2}(t_2)}{h_{B1}(-\infty)-h_{B2}(t_2)} - \frac{h^{*\prime}_{B2}(t_2)}{h^*_{B1}(0)-h^*_{B2}(t_2)} + \frac{h^{*\prime}_{B2}(t_2)}{h^*_{B1}(-\infty)-h^*_{B2}(t_2)} \\ &- \frac{h'_{A2}(t_2)}{h_{A1}(t_2)-h_{A2}(t_2)} + \frac{h'_{A2}(t_2)}{h_{A1}(0)-h_{A2}(t_2)} - \frac{h^{*\prime}_{A2}(t_2)}{h^*_{A1}(t_2)-h^*_{A2}(t_2)} + \frac{h^{*\prime}_{A2}(t_2)}{h^*_{A1}(0)-h^*_{A2}(t_2)}\,.\end{aligned} \tag{4.23}$$

From the first Eq. (4.6) we obtain

$$\begin{aligned}-\frac{\partial}{\partial t_1} g_A(t_1,t_2) = &-\mathcal{J}^2\int_{-\infty}^{0} dt_3\, e^{g_D(t_1,t_3)} - \mathcal{J}^2\int_{0}^{t_1} dt_3\, e^{g_{\tilde{A}}(t_1,t_3)} - 2\mathcal{J}^2\int_{t_1}^{t_2} dt_3\, e^{g_A(t_1,t_3)} \\ &+ \mathcal{J}^2\int_{-\infty}^{0} dt_3\, e^{g_B(t_3,t_1)} + \mathcal{J}^2\int_{0}^{t_1} dt_3\, e^{g_A(t_3,t_1)}\,.\end{aligned} \tag{4.24}$$

Inserting Eq. (4.11) into Eq. (4.24), we obtain

$$\begin{aligned}-\frac{h''_{A1}(t_1)}{h'_{A1}(t_1)} = &\frac{2h'_{A1}(t_1)}{h_{A2}(t_1)-h_{A1}(t_1)} \\ &- \frac{h^{*\prime}_{B2}(t_1)}{h^*_{B1}(0)-h^*_{B2}(t_1)} + \frac{h^{*\prime}_{B2}(t_1)}{h^*_{B1}(-\infty)-h^*_{B2}(t_1)} + \frac{h'_{B2}(t_1)}{h_{B1}(0)-h_{B2}(t_1)} - \frac{h'_{B2}(t_1)}{h_{B1}(-\infty)-h_{B2}(t_1)} \\ &+ \frac{h'_{A2}(t_1)}{h_{A1}(t_1)-h_{A2}(t_1)} - \frac{h'_{A2}(t_1)}{h_{A1}(0)-h_{A2}(t_1)} - \frac{h^{*\prime}_{A2}(t_1)}{h^*_{A1}(t_1)-h^*_{A2}(t_1)} + \frac{h^{*\prime}_{A2}(t_1)}{h^*_{A1}(0)-h^*_{A2}(t_1)}\,.\end{aligned} \tag{4.25}$$

From Eqs. (4.23) and (4.25) we obtain

$$\frac{h''_{A1}(t)}{h'_{A1}(t)} + \frac{h''_{A2}(t)}{h'_{A2}(t)} = 2\left(\frac{h'_{A1}(t)-h'_{A2}(t)}{h_{A1}(t)-h_{A2}(t)}\right)\,. \tag{4.26}$$

This is precisely the logarithmic derivative of the Majorana condition in Eq. (4.12). The compatibility condition at the boundary of region A and region B is

$$\frac{h'_{A1}(0)h'_{A2}(t_2)}{(h_{A1}(0)-h_{A2}(t_2))^2} = \frac{h'_{B1}(0)h'_{B2}(t_2)}{(h_{B1}(0)-h_{B2}(t_2))^2}\,. \tag{4.27}$$

This can be integrated to

$$\frac{h'_{A1}(0)}{h_{A2}(t_2)-h_{A1}(0)} = \frac{h'_{B1}(0)}{h_{B2}(t_2)-h_{B1}(0)} + c_4\,, \tag{4.28}$$

where c_4 is a constant of integration.

D. Combined equations

We adopt a simple choice to solve Eq. (4.28)

$$\begin{aligned}h_{B2}(t) &= h_{A2}(t)\,,\\ h_{B1}(0) &= h_{A1}(0)\,,\\ h'_{B1}(0) &= h'_{A1}(0)\,.\end{aligned} \tag{4.29}$$

Then we find that Eqs. (4.19) and (4.23) are consistent with each other. Collecting all equations, we need to solve

$$-\frac{h''_{A1}(t)}{h'_{A1}(t)} = -\frac{2h'_{A1}(t)}{h_{A1}(t)-h_{A2}(t)} + \frac{h^{*\prime}_{A2}(t)}{h^*_{B1}(-\infty)-h^*_{A2}(t)} - \frac{h'_{A2}(t)}{h_{B1}(-\infty)-h_{A2}(t)} + \frac{h'_{A2}(t)}{h_{A1}(t)-h_{A2}(t)} - \frac{h^{*\prime}_{A2}(t)}{h^*_{A1}(t)-h^*_{A2}(t)} \quad , \quad t \geq 0 \tag{4.30}$$

$$h'_{A1}(t)h'_{A2}(t) = -\mathcal{J}^2(h_{A1}(t)-h_{A2}(t))^2 \quad , \quad t \geq 0 \tag{4.31}$$

$$\frac{h'_{B2}(0)}{h_{B1}(t)-h_{B2}(0)} = \frac{h'_{B2}(0)}{h_{B1}(-\infty)-h_{B2}(0)} + \mathcal{J}^2 \int_{-\infty}^{t} dt'\, e^{g_C(t')} \quad , \quad t \leq 0 \tag{4.32}$$

$$h_{A1}(0) = h_{B1}(0)\,, \tag{4.33}$$

$$h'_{A1}(0) = h'_{B1}(0)\,, \tag{4.34}$$

$$h_{A2}(0) = h_{B2}(0)\,. \tag{4.35}$$

It can be verified that all expressions above are invariant SL(2,C) transformations of the $h_{\alpha 1}$ and $h_{\alpha 2}$ fields. Given the values of $h_{B1}(-\infty)$, $h_{B2}(0)$, $h'_{B2}(0)$, and $g_C(t)$, Eqs. (4.32-4.35) determine the values of $h_{A1}(0)$, $h'_{A1}(0)$, and $h_{A2}(0)$. Then Eqs. (4.30,4.31) uniquely determine $h_{A1}(t)$ and $h_{A2}(t)$ for all $t \geq 0$. Because of the SL(2,C) invariance, final result for $g_A(t_1,t_2)$ will be independent of the values chosen for $h_{B1}(-\infty)$, $h_{B2}(0)$, $h'_{B2}(0)$.

E. Exact solution

A solution of the form in Eq. (F16) does not apply to Eqs. (4.30-4.35) in region A because it does not have enough free parameters to satisfy the initial conditions. However, we can use the SL(2,C) invariance of Eqs. (4.30-4.32) to propose the following ansatz:

$$h_{A1}(t) = \frac{a\,e^{\sigma t}+c}{c\,e^{\sigma t}+d} \quad , \quad h_{A2}(t) = \frac{a\,e^{-2i\theta}e^{\sigma t}+b}{c\,e^{-2i\theta}e^{\sigma t}+d}\,. \tag{4.36}$$

We can now verify that Eq. (4.36) is an exact solution of Eqs. (4.30-4.35). This solution is characterized by 4 complex numbers a, b, c, d and two real numbers θ, σ. These are uniquely determined from the values of $h_{B1}(-\infty)$, $h_{A1}(0)$, $h'_{A1}(0)$, and $h_{A2}(0)$ by the solution of the

following 6 equations

$$
\begin{aligned}
ad - bc &= 1\,, \\
\sigma &= 2\mathcal{J}\sin(\theta)\,, \\
e^{-4i\theta} &= \frac{(b - d\,h_{B1}(-\infty))(a^* - c^*\,h^*_{B1}(-\infty))}{(b^* - d^*\,h^*_{B1}(-\infty))(a - c\,h_{B1}(-\infty))}\,, \\
h_{A1}(0) &= \frac{a+b}{c+d}\,, \\
h_{A2}(0) &= \frac{a\,e^{-2i\theta} + b}{c\,e^{-2i\theta} + d}\,, \\
h'_{A1}(0) &= \frac{2\sin(\theta)}{(c+d)^2}\,.
\end{aligned}
\tag{4.37}
$$

Inserting Eq. (4.36) into Eq. (4.11) we obtain the exact solution for the Green's function in region A

$$
g_A(t_1, t_2) = \ln\left[\frac{-\sigma^2}{4\mathcal{J}^2\sinh^2(\sigma(t_1 - t_2)/2 + i\theta)}\right]\,. \tag{4.38}
$$

As expected from SL(2, C) invariance, this result is independent of the values of a, b, c, d. Moreover, as stated in Section I, the surprising feature of this result is that it only depends *only* upon the relative time t, and is independent of $\mathcal{T} = (t_1 + t_2)/2$. Indeed Eq. (4.38) obeys a KMS condition [12, 22] for an inverse temperature

$$
\beta_f = \frac{2(\pi - 2\theta)}{\sigma}\,; \tag{4.39}
$$

we can verify the value in Eq. (4.39) by taking a Fourier transform of Eq. (4.38) and comparing with Eq. (3.3). So we obtain our main result of the large q limit: all of quadrant A is in thermal equilibrium at the temperature β_f. We also numerically integrated Eqs. (4.30-4.35), starting from generic initial conditions, and verified that the numerical solution obeyed the expressions in Eqs. (4.36) and (4.37). The equations in Eq. (4.37) determine the values of σ and θ in the final state, and hence the value of the final temperature via Eq. (4.39). In general, this will be different from the value of the initial temperature in quadrant C.

Eqs. (4.36) and (4.37) also determine the solutions in the other quadrants via the expressions specified earlier. The solutions in region $\widetilde{A}$ follow from the conjugacy property in Eq. (4.16). In quadrant B, we have $h_{B2}(t) = h_{A2}(t)$ in Eq. (4.29), while $h_{B1}(t)$ was specified in Eq. (4.21) using the initial state in quadrant C. Note that the solution in quadrant B is not of a thermal form, as h_{B1} and h_{B2} are not simply related as in Eq. (4.36). The solution

in quadrant D follows from that in quadrant B via the conjugacy property in Eq. (4.16). Finally, the initial state in quadrant C was described in Appendix F.

Note also that in the limit $\beta_f \mathcal{J} \gg 1$, we have $\theta \ll 1$ and then

$$\sigma = \frac{2\pi}{\beta_f} \,. \tag{4.40}$$

Then Eqs. (4.1) and (4.38) describe the $1/q$ expansion of the low temperature conformal solution [22] describing the equilibrium non-Fermi liquid state (see Appendix B). And the value of σ in Eq. (4.40) is the maximal Lyapunov exponent for quantum chaos [25]. This chaos exponent appears in the time evolution of $h_{1,2}(t)$. However, in the large q limit, it does not directly control the rapid thermalization rate. We note that recent studies of Fermi surfaces coupled to gauge fields, and of disordered metals, also found a relaxation/dephasing rate which was larger than the Lyapunov rate [26, 27].

V. CONCLUSIONS

Quantum many-body systems without quasiparticle excitations are expected to locally thermalize in the fastest possible times of order $\hbar/(k_B T)$ as $T \to 0$, where T is the absolute temperature of the final state [18]. This excludes *e.g.* the existence of systems in which the local thermalization rate, $\Gamma \sim T^p$ as $T \to 0$ with $p < 1$, and no counterexamples have been found.

In this paper we examined SYK models, which saturate the more rigorous bound on the Lyapunov exponent characterizing the rate of growth of chaos in quantum systems [25]. Our numerical study of the model with a final Hamiltonian with $q = 4$ showed that this system does thermalize rapidly, and the thermalization rate is consistent with $\Gamma = CT$ at low T where C is dimensionless constant, as indicated in Eq. (1.10) and Fig. 3.

We also studied a large q limit of the SYK models, where an exact analytic solution of the non-equilibrium dynamics was possible. Here we found that thermalization of the fermion Green's function was instantaneous.

Remarkably, the large q solution given by Eq. (4.11) and (4.36): also has a direct connection with the Schwarzian. The Schwarzian was proposed as an effective Lagrangian for the low energy limit of the equilibrium theory of the SYK model. Consider the Euler-Lagrange

equation of motion of a Lagrangian, $\mathcal{L}$, which is the Schwarzian of $h(t)$

$$\mathcal{L}[h(t)] = \frac{h'''(t)}{h'(t)} - \frac{3}{2}\left(\frac{h''(t)}{h'(t)}\right)^2 . \tag{5.1}$$

The equation of motion is

$$[h'(t)]^2 h''''(t) + 3\,[h''(t)]^3 - 4h'(t)h''(t)h'''(t) = 0\,. \tag{5.2}$$

It can now be verified that the expressions for $h_{1,2}(t)$ in Eq. (4.36) both obey Eq. (5.2), with the parameter σ controlling the exponential growth of $h_{1,2}(t)$. (Note, however, that we did not obtain Eq. (4.36) by solving Eq. (5.2): instead, Eq. (4.36) was obtained by solving the Kadanoff-Baym equations for the large-q SYK model in Eq. (4.6).) The structure of $h_{1,2}(t)$ in Eq. (4.36) is intimately connected to the SL(2,C) invariance and the instantaneous thermalization of the large q limit. The connection with the Schwarzian here indicates that gravitational models [11–17] of the quantum quench in AdS_2, which map to a Schwarzian boundary theory, also exhibit instant thermalization.

Indeed, the equation of motion of the metric in two-dimensional gravity [15] takes a form identical to that for the two-point fermion correlator in Eq. (4.10). Studies of black hole formation in AdS_2 from a collapsing shell of matter show that the Hawking temperature of the black hole jumps instantaneously to a new equilibrium value after the passage of the shell [17, 28]. These features are strikingly similar to those obtained in our large q analysis. There have been studies of quantum quenches in AdS_2, either in the context of quantum impurity problems [29], or in the context of higher-dimensional black holes which have an AdS_2 factor in the low energy limit [30]; it would be useful to analytically extract the behavior of just AdS_2 by extending such studies.

The final question we must ask is the following: what do our results tell us about the overall thermalization process in the SYK model? In this paper we have studied the thermalization of the Green's function, which is the simplest object we could have picked. We found that the thermalization was instantaneous in the large q limit, but finite for general q. In order to reconcile the large q limit with numerical results it will be necessary to study higher order corrections in $1/q$ to understand how this connects to the numerical $q = 4$ numerical solution: does the constant $C \to \infty$ as $q \to \infty$, or (as pointed to us by Aavishkar Patel) is thermalization at large q a two-step process. In two-step scenario, we have a very rapid pre-thermalization of the two point function (which we have computed) is followed by a slower true thermalization of higher order corrections.

We thank J. Maldacena of informing us about another work [31] which studied aspects of thermalization of SYK models by very different methods, along with connections to gravity in AdS_2. Sonner and Velma [32] demonstrated that the SYK model obeys eigenstate thermalization. Gu *et al.* [33] studied an SYK chain for a thermofield double initial state, and found prethermalization behavior.

ACKNOWLEDGMENTS

We would like to thank Yingfei Gu, Wenbo Fu, Daniel Jafferis, Michael Knapp, Juan Maldacena, Ipsita Mandal, Thomas Mertens, Robert Myers, Aavishkar Patel, Stephen Shenker, and Herman Verlinde for valuable discussions. AE acknowledges support from the German National Academy of Sciences Leopoldina through grant LPDS 2014-13. AE would like to thank the Erwin Schrödinger International Institute for Mathematics and Physics in Vienna, Austria, for hospitality and financial support during the workshop on "Synergies between Mathematical and Computational Approaches to Quantum Many-Body Physics". VK acknowledges support from the Alexander von Humboldt Foundation through a Feodor Lynen Fellowship. JS was supported by the National Science Foundation Graduate Research Fellowship under Grant No. DGE1144152. This research was supported by the NSF under Grant DMR-1360789 and DMR-1664842, and MURI grant W911NF-14-1-0003 from ARO. Research at Perimeter Institute is supported by the Government of Canada through Industry Canada and by the Province of Ontario through the Ministry of Economic Development & Innovation. SS also acknowledges support from Cenovus Energy at Perimeter Institute.

Appendix A: Spectral function and Green's functions of random hopping model

The random hopping model of Majorana fermions, *i. e.*the SYK Hamiltonian for $q = 2$, is exactly solvable [12]. The Matsubara Green's function follows from the solution of the Dyson equation

$$G(i\omega_n)^{-1} = i\omega_n - \Sigma(i\omega_n) = i\omega_n + J_2^2 G(i\omega_n). \tag{A1}$$

This can be rewritten as a quadratic equation for $\big(G(i\omega_n)\big)^{-1}$. Matching the branches with the correct high-frequency asymptotics and symmetry yields the propagator

$$G(i\omega_n) = \frac{2}{i\omega_n + i\,\mathrm{sgn}(\omega_n)\sqrt{\omega_n^2 + 4J_2^2}}. \tag{A2}$$

Analytically continuing to the real frequency axis from the upper half plane yields the retarded Green's function,

$$G^R(\omega + i\delta) = \frac{2}{\omega + i\delta + i\sqrt{4J_2^2 - (\omega + i\delta)^2}}, \tag{A3}$$

where δ can be set to zero due to the presence of the finite imaginary part and $\mathrm{sgn}\,\omega_n \to 1$ in the analytic continuation from the upper half plane. For the spectral function, we obtain

$$A(\omega) = -2\,\mathrm{Im}\,G^R(\omega + i\delta) = \frac{2}{J_2}\sqrt{1 - \Big(\frac{\omega}{2J_2}\Big)^2} \qquad \text{for } |\omega| < 2J_2, \tag{A4}$$

which is the well-known semicircular density of states.

This yields the following expression for $G^>(t)$

$$iG^>(t) = \frac{1}{2J_2 t}\big(J_1(2J_2 t) - iH_1(2J_2 t)\big), \tag{A5}$$

where J_1 is the Bessel function of the first kind (`BesselJ` in `Mathematica`) and H_1 is the Struve function (`StruveH` in `Mathematica`).

Appendix B: Spectral Function in the Conformal Limit

In the scaling limit at non-zero temperature the retarded Green's function is given by the following expression

$$iG^R(t) = 2b(\cos\pi\Delta)\left(\frac{\pi}{\beta\sinh\frac{\pi t}{\beta}}\right)^{2\Delta}\theta(t)\,, \tag{B1}$$

where $\Delta = 1/q$ is the fermion scaling dimension. At $q = 4$ we obtain

$$iG_c^R(t) = \sqrt{2}b\left(\frac{\pi}{\beta\sinh\frac{\pi t}{\beta}}\right)^{\frac{1}{2}}\theta(t) \tag{B2}$$

The Wigner transform of the retarded Green's functions is given by

$$\begin{aligned} iG^R(\omega) &= \sqrt{2}b\int_0^\infty dt e^{i\omega t}\left(\frac{\pi}{\beta\sinh\frac{\pi t}{\beta}}\right)^{\frac{1}{2}} \\ &= b\left(\frac{\pi}{\beta}\right)^{-\frac{1}{2}} B\left(\frac{1}{2}; \frac{1}{4} - \frac{i\beta\omega}{2\pi}\right)\,, \end{aligned} \tag{B3}$$

where $b = (4\pi J_4^2)^{-1/4}$. The associated spectral function is

$$A(\mathcal{T}, \omega) = 2b \left(\frac{\pi}{\beta}\right)^{-\frac{1}{2}} \mathrm{Re}\left[B\left(\frac{1}{2}; \frac{1}{4} - \frac{i\beta\omega}{2\pi}\right)\right] . \tag{B4}$$

Appendix C: Details on the Numerical Solution of Kadanoff-Baym equation

The Green's function is typically determined on two-dimensional grids in (t, t') space with 8000×8000 or 12000×12000 points, where the quench happens after half of the points in each direction. When starting from initial states in which only J_2 is finite, the Green's function decays algebraically in time. This leads to significant finite size effects in Fourier transforms. In order to reduce the latter, most numerical results were obtained by starting from a thermal state in which J_2 and J_4, or only J_4, are finite. In these cases, the Green's function decays exponentially as a function of the relative time dependence.

We checked the quality and consistency of the results by monitoring the conservation of energy, the normalization of the spectral function and the real and imaginary part of the retarded propagator are Kramers-Kronig consistent for long times after the quench.

In order to time-evolve the Kadanoff-Baym equations we have to determine $G^<(t_1, t_2)$ for t_1, t_2. When quenching the ground state of the random hopping model, we can use the exact solution for $G^>$ as initial condition. When we do not have an analytic expression the Green's function we solve the Dyson equation self-consistently according to the following scheme:

1. Prepare $iG^>$ with an initial guess, for example the propagator of the random hopping model.

2. Computation of retarded self-energy in time domain:

$$i\Sigma^R(t) = \Theta(t)(i\Sigma^>(t) + i\Sigma^>(-t)) \tag{C1}$$

3. Fourier transformation

$$i\Sigma^R(\omega) = \int_{-\infty}^{\infty} dt e^{i\omega t} i\Sigma^R(t) \tag{C2}$$

4. Solve the Dyson equation:

$$G^R(\omega) = \frac{1}{\omega - \Sigma^R(\omega)} \tag{C3}$$

5. Determine spectral function

$$A(\omega) = -2\,\mathrm{Im}\,G^R(\omega) \tag{C4}$$

6. Determine $iG^>(\omega)$ from spectral function,

$$iG^>(\omega) = (1 - n_F(\omega))A(\omega) \tag{C5}$$

Note that this is the only step in the self-consistency procedure where the temperature β^{-1} enters through the Fermi function n_F.

7. Fourier transformation to the time domain

$$iG^>(t) = \int_{-\infty}^{\infty} \frac{d\omega}{2\pi} e^{-i\omega t} iG^>(\omega) \tag{C6}$$

8. Continue with step 2 until convergence is reached.

Appendix D: Numerical quenches: simpler cases

This appendix describes the quenches A-C discussed in Section III.

1. $(J_{2,i}, 0) \to (J_{2,f}, 0)$ quench: Rescaling of the Random-Hopping model

We start by discussing the simplest quench protocol A. In Fig. 5 we show the spectral function long before and long after a parameter quench. These results were obtained from a numerical Fourier transformation of the retarded Green's function as described by Eq. (3.6) with a broadening of $\delta = 0.025$. In Fig. 6, we show the frequency dependence of the Keldysh component of the fermionic Green's function for the same quench protocol as in Fig. 5. We determined the inverse temperature β using Eq. (3.8), and found that βJ_2 was roughly constant across the quench. All three results of this $(J_{2,i}, 0) \to (J_{2,f}, 0)$ quench are consistent with a rescaling of energy scales for all quantities. This is expected because the random hopping model has only one energy scale J_2, and the analog of the reparameterization in Eq. (4.5) applies here. This also applies to the complementary case $(0, J_{4,i}) \to (0, J_{4,f})$ (as was pointed out to us by J. Maldacena). For analytic expressions of the spectral functions we refer to Appendix A.

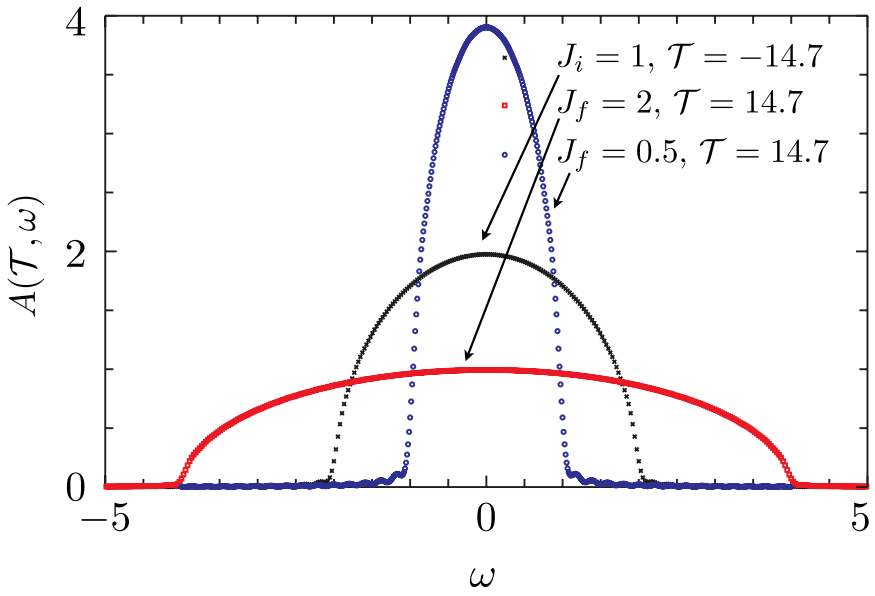

FIG. 5. The spectral function of the random hopping model A long before ($\mathcal{T} = -14.7$) and after ($\mathcal{T} = 14.7$) a parameter quench from $J_{2,i} = 1$ to $J_{2,f} = 0.5$ and 2.0. The width depends only on the value of J_f, becoming wider if $J_f > J_i$ and narrower if $J_f < J_i$.

2. $(0, 0) \to (0, J_4)$ quench: From bare Majorana fermions to the SYK model

Next we conside the quench B. In Fig. 7, we show the spectral function long after suddely switching on the quartic interaction in the SYK model, starting from bare, noninteracting Majorana fermions. When interpreting results of this quench protocol, it is important to keep in mind that the Hamiltonian before the quench is zero, so that any finite $J_{4,f}$ is an arbitrarily strong perturbation. We found that the total energy is zero both before and after the quench, *i. e.* the quench does not pump energy into the system, and that the Keldysh component of the Green's function vanishes before and after the quench. The latter is to be expected for free Majorana fermions, and is consistent with the post-quench temperature of the system being infinite, *i. e.* $\beta_f = 0$. Indeed the spectral function in Fig. 7 agrees with that of the SYK model at infinite temperature.

3. $(J_{2,i}, 0) \to (0, J_{4,f})$: From a quadratic to a quartic model

We now consider C, the model containing both $q = 2$ and $q = 4$ interactions. The quench from the purely quadratic to the purely quartic model decouples the regions $t_1, t_2 < 0$ from

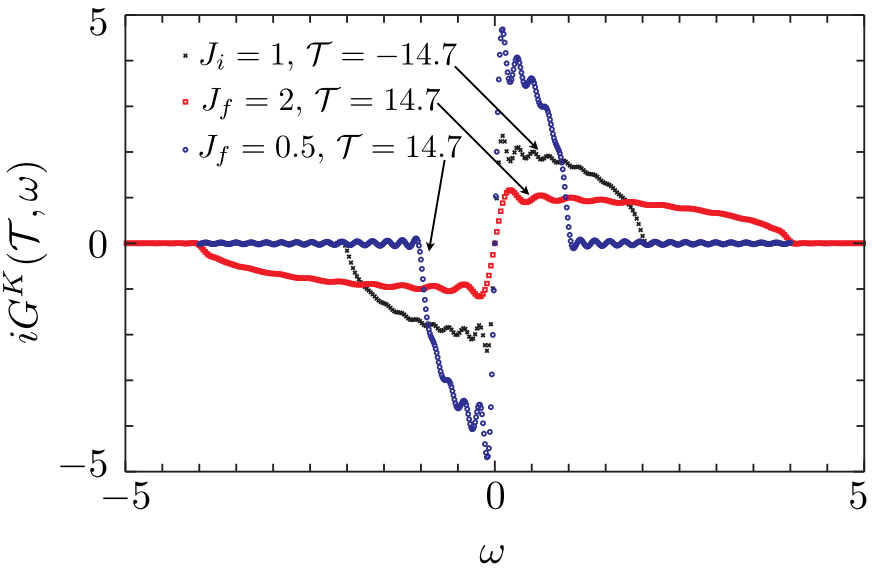

FIG. 6. The Keldysh component of the Green's function of the random hopping model A long before ($\mathcal{T} = -14.7$) and after ($\mathcal{T} = 14.7$) a parameter quench from $J_{2,i} = 1$ to $J_{2,f} = 0.5$ and 2.0.

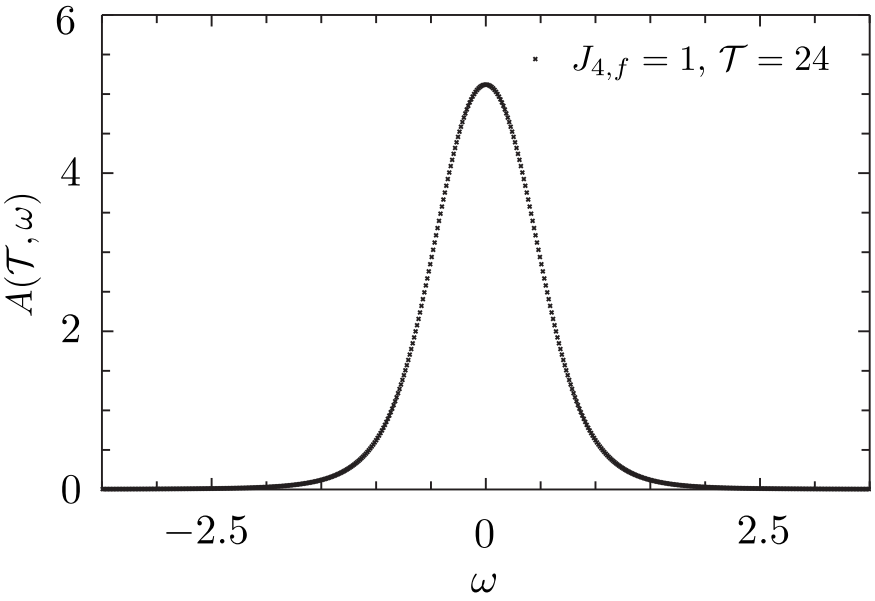

FIG. 7. The spectral function for Majorana fermions is shown long after a quench starting with free Majorana fermions and switching on a $q = 4$ SYK interaction term. Here $J_{4,f} = 1$.

$t_1, t_2 > 0$: this can be seen from the structure of the Kadanoff-Baym equations, and of the self-energy for this quench protocol, which reads

$$\Sigma(t_1, t_2) = \Theta(-t_1)\Theta(-t_2)J_2^2 G(t_1, t_2) - \Theta(t_1)\Theta(t_2)J_4^2 G(t_1, t_2)^3 \,. \tag{D1}$$

Inserting this into the Kadanoff-Baym equations for $t_1 > 0$ and $t_2 > 0$, we can see that all time integrals are restricted to positive times, and the initial condition does not matter. Although $G^>(t_1, t_2)$ shows some time evolution for $t_1 \gtrsim 0$ and $t_2 \lesssim 0$ due to integrals involving the region with $t_1 < 0$ and $t_2 < 0$, $G^>$ in this region does not influence the time evolution at positive t_1, t_2 because $\Sigma(t_1, t_2) = 0$ when $t_1 \gtrsim 0$ and $t_2 \lesssim 0$. Thus, the relevant initial condition for the time evolution of $G^>(t_1, t_2)$ is $iG^>(t_1 = 0, t_2 = 0) = 1/2$. Hence propagating $iG^>$ forward in time using the self-energy of the quartic model, we obtain the same time evolution at positive times as we did when starting from bare Majorana fermions in case B. So the final state here is also the SYM model at infinite temperature.

Appendix E: Conjugacy property of $g(t_1, t_2)$

In this appendix we illustrate that the causality structure of the Kadanoff-Baym equations eq. (4.6) leads to the property

$$[g(t_1, t_2)]^* = g(t_2, t_1) \tag{E1}$$

in all four quadrants of Fig. 8. Since the system is thermal in quadrant C the conjugacy

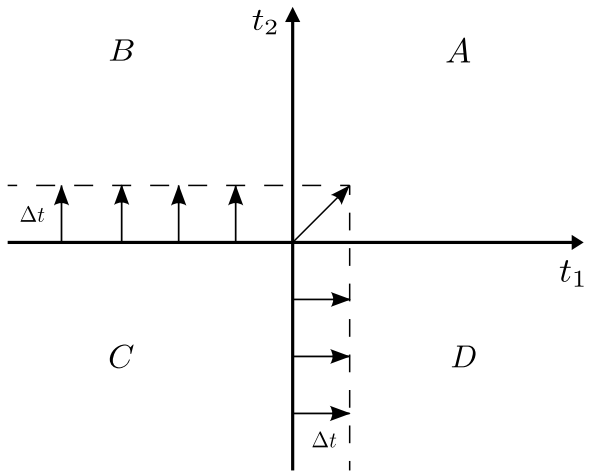

FIG. 8. The propagation of the conjugacy property in the t_1-t_2 plane.

property $[g(t_1, t_2)]^* = g(t_2, t_1)$ can be read off the thermal solution for $t_1, t_2 \leq 0$. Next, we consider the propagation from the line $\{(t_1, t_2) \in \mathbb{R}^2 \,|t_2 = 0, t_1 \leq 0\}$ for an infinitesimal time Δt in the t_2 direction to the line $\{(t_1, t_2) \in \mathbb{R}^2 \,|t_2 = \Delta t, t_1 \leq 0\}$. We discretize equation (4.6)

as follows

$$\frac{1}{\Delta t}\left[g(t_1,\Delta t)-g(t_1,0)\right]=2\int_{-\infty}^{t_1}dt_3\,\mathcal{J}(t_3)\mathcal{J}(0)e^{g(t_3,0)}-\int_{-\infty}^{0}dt_3\,\mathcal{J}(t_3)\mathcal{J}(0)\left[e^{g(t_3,0)}+e^{g(0,t_3)}\right]$$
$$+2\int_{-\infty}^{t_1}dt_3\,\mathcal{J}_p(t_3)\mathcal{J}_p(0)e^{pg(t_3,0)}-\int_{-\infty}^{0}dt_3\,\mathcal{J}_p(t_3)\mathcal{J}_p(0)\left[e^{pg(t_3,0)}+e^{pg(0,t_3)}\right] \tag{E2}$$

and solve the resulting equation for $g(t_1,\Delta t)$. Taking the complex conjugate leads to

$$g(t_1,\Delta t)^*=g(t_1,0)^*+\Delta t\left\{2\int_{-\infty}^{t_1}dt_3\,\mathcal{J}(t_3)\mathcal{J}(0)e^{g(t_3,0)^*}-\int_{-\infty}^{0}dt_3\,\mathcal{J}(t_3)\mathcal{J}(0)\left[e^{g(t_3,0)^*}+e^{g(0,t_3)^*}\right]\right.$$
$$\left.+2\int_{-\infty}^{t_1}dt_3\,\mathcal{J}_p(t_3)\mathcal{J}_p(0)e^{pg(t_3,0)^*}-\int_{-\infty}^{0}dt_3\,\mathcal{J}_p(t_3)\mathcal{J}_p(0)\left[e^{pg(t_3,0)^*}+e^{pg(0,t_3)^*}\right]\right\}. \tag{E3}$$

On the right hand side we are allowed to use the property $g(t_1,t_2)^*=g(t_2,t_1)$ since all g's are still living in the C quadrant. We obtain

$$g(t_1,\Delta t)^*=g(0,t_1)+\Delta t\left\{2\int_{-\infty}^{t_1}dt_3\,\mathcal{J}(t_3)\mathcal{J}(0)e^{g(0,t_3)}-\int_{-\infty}^{0}dt_3\,\mathcal{J}(t_3)\mathcal{J}(0)\left[e^{g(0,t_3)}+e^{g(t_3,0)}\right]\right.$$
$$\left.+2\int_{-\infty}^{t_1}dt_3\,\mathcal{J}_p(t_3)\mathcal{J}_p(0)e^{pg(0,t_3)}-\int_{-\infty}^{0}dt_3\,\mathcal{J}_p(t_3)\mathcal{J}_p(0)\left[e^{pg(0,t_3)}+e^{pg(t_3,0)}\right]\right\}. \tag{E4}$$

Next we let the system propagate from the line $\{(t_1,t_2)\in\mathbb{R}^2\,|t_2\leq 0,t_1=0\}$ for an infinitesimal time Δt in the t_1 direction to the line $\{(t_1,t_2)\in\mathbb{R}^2\,|t_1=\Delta t,t_2\leq 0\}$. We discretize equation (4.3) as follows

$$-\frac{1}{\Delta t}\left[g(\Delta t,t_2)-g(0,t_2)\right]=\int_{-\infty}^{0}dt_3\,\mathcal{J}(0)\mathcal{J}(t_3)\left[e^{g(0,t_3)}+e^{g(t_3,0)}\right]-2\int_{-\infty}^{t_2}dt_3\,\mathcal{J}(0)\mathcal{J}(t_3)e^{g(0,t_3)}$$
$$+\int_{-\infty}^{0}dt_3\,\mathcal{J}_p(0)\mathcal{J}_p(t_3)\left[e^{pg(0,t_3)}+e^{pg(t_3,0)}\right]-2\int_{-\infty}^{t_2}dt_3\,\mathcal{J}_p(0)\mathcal{J}_p(t_3)e^{pg(0,t_3)} \tag{E5}$$

We set $t_2=t_1$ in the last equation and solve for $g(\Delta t,t_1)$ leading to

$$g(\Delta t,t_1)=g(0,t_1)-\Delta t\left\{\int_{-\infty}^{0}dt_3\,\mathcal{J}(0)\mathcal{J}(t_3)\left[e^{g(0,t_3)}+e^{g(t_3,0)}\right]-2\int_{-\infty}^{t_1}dt_3\,\mathcal{J}(0)\mathcal{J}(t_3)e^{g(0,t_3)}\right.$$
$$\left.+\int_{-\infty}^{0}dt_3\,\mathcal{J}_p(0)\mathcal{J}_p(t_3)\left[e^{pg(0,t_3)}+e^{pg(t_3,0)}\right]-2\int_{-\infty}^{t_1}dt_3\,\mathcal{J}_p(0)\mathcal{J}_p(t_3)e^{pg(0,t_3)}\right\}. \tag{E6}$$

Comparing the right hand side of (E3) with (E6) we conclude $g(t_1, \Delta t)^* = g(\Delta t, t_1)$. Furthermore, the point $g(\Delta t, \Delta t)$ fulfills the conjugate property trivially. In total we propagated the conjugate property one time slice. Repeating this argument for every time slice of size Δt, the property will hold in all four quadrants of Fig. 8.

Appendix F: Initial state in the large q limit

In quadrant C in Fig. 4, all Green's functions are dependent only on time differences, so we can write

$$g_C(t_1, t_2) \equiv g_C(t_1 - t_2) \tag{F1}$$

and Eq. (4.6) as

$$\frac{dg_C(t)}{dt} = \mathcal{J}^2 \int_{-\infty}^{\infty} dt'\, e^{g_C(t')}\, \mathrm{sgn}(t'-t) + \mathcal{J}_p^2 \int_{-\infty}^{\infty} dt'\, e^{pg_C(t')}\, \mathrm{sgn}(t'-t)\,. \tag{F2}$$

This implies the second order differential equation (also obtainable from Eq. (4.8))

$$-\frac{d^2 g_C}{dt^2} = 2\mathcal{J}^2 e^{g_C} + 2\mathcal{J}_p^2 e^{pg_C}\,. \tag{F3}$$

Eq. (F3) turns out to be exactly solvable at $p = 2$ (pointed out to us by Wenbo Fu, following [34]). Inserting $g_C(t) = \ln(-1/f(t))$ into Eq. (F3) we get

$$\frac{1}{f}\frac{d^2 f}{dt^2} - \frac{1}{f^2}\left(\frac{df}{dt}\right)^2 = -\frac{2\mathcal{J}^2}{f} + \frac{2\mathcal{J}_2^2}{f^2} \tag{F4}$$

The solution of this differential equation yields

$$g_C(t) = \ln\left[\frac{-\sigma^2}{\sqrt{4\mathcal{J}^4 + 2\mathcal{J}_2^2\sigma^2}\cosh(\sigma t - 2i\theta) - 2\mathcal{J}^2}\right], \tag{F5}$$

with

$$\cos(2\theta) = \frac{2\mathcal{J}^2 - \sigma^2}{\sqrt{4\mathcal{J}^4 + 2\mathcal{J}_2^2\sigma^2}}\,. \tag{F6}$$

By evaluating the Fourier transform of the Green's function we find $G^>(-\omega) = e^{-\beta_i\omega}G^>(\omega)$, or by analytically continuing to imaginary time, we find that the initial inverse temperature is

$$\beta_i = \frac{2(\pi - 2\theta)}{\sigma}\,. \tag{F7}$$

We will ultimately be interested in the scaling limit in which $\theta \to 0$ and $\sigma \ll \mathcal{J}, \mathcal{J}_2$.

Eq. (F3) is also exactly solvable at $p = 1/2$ by

$$g_C(t) = 2\ln\left[\frac{\sigma^2/2}{i\sqrt{4\mathcal{J}_{1/2}^4 + \mathcal{J}^2\sigma^2}\sinh(\sigma t/2 - i\theta) + 2\mathcal{J}_{1/2}^2}\right], \tag{F8}$$

where now

$$\sin(\theta) = \frac{\sigma^2/2 - 2\mathcal{J}_{1/2}^2}{\sqrt{4\mathcal{J}_{1/2}^4 + \mathcal{J}^2\sigma^2}}. \tag{F9}$$

The value of the inverse initial temperature remains as in Eq. (F7).

Note that both solutions in Eqs. (F5) and (F8) obey

$$g_C(-t) = g_C^*(t) \tag{F10}$$

It is also useful to recast the solution in quadrant C for the case $\mathcal{J}_p = 0$ in the form of Eq. (4.11). We subdivide quadrant C into two subregions just as in quadrant A. From Eqs. (4.6) and (4.11) we obtain for $t_2 > t_1$

$$\begin{aligned}
\frac{h''_{C1}(t_1)}{h'_{C1}(t_1)} &= \frac{2h^{*\prime}_{C2}(t_1)}{h^*_{C1}(t_1) - h^*_{C2}(t_1)} - \frac{2h^{*\prime}_{C2}(t_1)}{h^*_{C1}(-\infty) - h^*_{C2}(t_1)} - \frac{2h'_{C1}(t_1)}{h_{C2}(t_1) - h_{C1}(t_1)} \\
&\quad - \frac{h^{*\prime}_{C2}(t_1)}{h^*_{C1}(t_1) - h^*_{C2}(t_1)} + \frac{h^{*\prime}_{C2}(t_1)}{h^*_{C1}(-\infty) - h^*_{C2}(t_1)} - \frac{h'_{C2}(t_1)}{h_{C1}(t_1) - h_{C2}(t_1)} + \frac{h'_{C2}(t_1)}{h_{C1}(-\infty) - h_{C2}(t_1)} \\
\frac{h''_{C2}(t_2)}{h'_{C2}(t_2)} &= -\frac{2h'_{C2}(t_2)}{h_{C1}(-\infty) - h_{C2}(t_2)} - \frac{h'_{C2}(t_2)}{h_{C1}(t_2) - h_{C2}(t_2)} + \frac{h'_{C2}(t_2)}{h_{C1}(-\infty) - h_{C2}(t_2)} \\
&\quad - \frac{h^{*\prime}_{C2}(t_2)}{h^*_{C1}(t_2) - h^*_{C2}(t_2)} + \frac{h^{*\prime}_{C2}(t_2)}{h^*_{C1}(-\infty) - h^*_{C2}(t_2)}.
\end{aligned} \tag{F11}$$

Adding the equations in Eq. (F11), we have

$$\frac{h''_{C1}(t)}{h'_{C1}(t)} + \frac{h''_{C2}(t)}{h'_{C2}(t)} = 2\left(\frac{h'_{C1}(t) - h'_{C2}(t)}{h_{C1}(t) - h_{C2}(t)}\right) \tag{F12}$$

which integrates to the expected

$$h'_{C1}(t)h'_{C2}(t) = -\mathcal{J}^2(h_{C1}(t) - h_{C2}(t))^2 \tag{F13}$$

The final equations for the thermal equilibrium state are

$$\begin{aligned}
\frac{h''_{C1}(t)}{h'_{C1}(t)} &= \frac{2h'_{C1}(t_1)}{h_{C1}(t) - h_{C2}(t)} - \frac{h^{*\prime}_{C2}(t)}{h^*_{C1}(-\infty) - h^*_{C2}(t)} + \frac{h'_{C2}(t)}{h_{C1}(-\infty) - h_{C2}(t)} \\
&\quad - \frac{h'_{C2}(t)}{h_{C1}(t) - h_{C2}(t)} + \frac{h^{*\prime}_{C2}(t)}{h^*_{C1}(t) - h^*_{C2}(t)}
\end{aligned} \tag{F14}$$

$$h'_{C1}(t)h'_{C2}(t) = -\mathcal{J}^2(h_{C1}(t) - h_{C2}(t))^2. \tag{F15}$$

Unlike Eqs. (4.30,4.31), Eqs. (F14,F15) have to be integrated from $t = -\infty$. One solution of Eqs. (F14,F15) is

$$h_{C1}(t) = h_{C1}(-\infty) + Ae^{i\theta}e^{\sigma t} \qquad h_{C2}(t) = h_{C1}(-\infty) + Ae^{-i\theta}e^{\sigma t} \tag{F16}$$

with

$$\sigma = 2\mathcal{J}\sin(\theta)\,. \tag{F17}$$

Note that the $g_C(t_1, t_2)$ obtained from this solution agrees with Eq. (F5) at $\mathcal{J}_2 = 0$ and with Eq. (F8) at $\mathcal{J}_{1/2} = 0$.

---

[1] J. H. Traschen and R. H. Brandenberger, "Particle production during out-of-equilibrium phase transitions," Phys. Rev. D **42**, 2491 (1990).

[2] L. McLerran and R. Venugopalan, "Computing quark and gluon distribution functions for very large nuclei," Phys. Rev. D **49**, 2233 (1994).

[3] E. Goulielmakis, V. S. Yakovlev, A. L. Cavalieri, M. Uiberacker, V. Pervak, A. Apolonski, R. Kienberger, U. Kleineberg, and F. Krausz, "Attosecond control and measurement: Light-wave electronics," Science **317**, 769 (2007).

[4] A. Polkovnikov, K. Sengupta, A. Silva, and M. Vengalattore, "Colloquium: Nonequilibrium dynamics of closed interacting quantum systems," Rev. Mod. Phys. **83**, 863 (2011), arXiv:1007.5331 [cond-mat.stat-mech].

[5] T. Kinoshita, T. Wenger, and D. S. Weiss, "A quantum Newton's cradle," Nature **440**, 900 (2006).

[6] J. Berges, S. Borsányi, and C. Wetterich, "Prethermalization," Phys. Rev. Lett. **93**, 142002 (2004), hep-ph/0403234.

[7] A. Kamenev, *Field Theory of Non-Equilibrium Systems*, 3rd ed. (Cambridge University Press, Cambridge, 2013).

[8] K. Damle and S. Sachdev, "Nonzero-temperature transport near quantum critical points," Phys. Rev. B **56**, 8714 (1997), cond-mat/9705206.

[9] S. Sachdev, "Nonzero-temperature transport near fractional quantum Hall critical points," Phys. Rev. B **57**, 7157 (1998), cond-mat/9709243.

[10] S. Sachdev and J. Ye, "Gapless spin-fluid ground state in a random quantum Heisenberg magnet," Phys. Rev. Lett. **70**, 3339 (1993), cond-mat/9212030.

[11] A. Y. Kitaev, "Talks at KITP, University of California, Santa Barbara," Entanglement in Strongly-Correlated Quantum Matter (2015).

[12] J. Maldacena and D. Stanford, "Remarks on the Sachdev-Ye-Kitaev model," Phys. Rev. D **94**, 106002 (2016), arXiv:1604.07818 [hep-th].

[13] S. Sachdev, "Holographic metals and the fractionalized Fermi liquid," Phys. Rev. Lett. **105**, 151602 (2010), arXiv:1006.3794 [hep-th].

[14] S. Sachdev, "Strange metals and the AdS/CFT correspondence," J. Stat. Mech. **1011**, P11022 (2010), arXiv:1010.0682 [cond-mat.str-el].

[15] A. Almheiri and J. Polchinski, "Models of AdS_2 backreaction and holography," JHEP **11**, 014 (2015), arXiv:1402.6334 [hep-th].

[16] K. Jensen, "Chaos and hydrodynamics near AdS_2," Phys. Rev. Lett. **117**, 111601 (2016), arXiv:1605.06098 [hep-th].

[17] J. Engelsöy, T. G. Mertens, and H. Verlinde, "An investigation of AdS_2 backreaction and holography," JHEP **07**, 139 (2016), arXiv:1606.03438 [hep-th].

[18] S. Sachdev, *Quantum Phase Transitions*, 1st ed. (Cambridge University Press, Cambridge, UK, 1999).

[19] M. Babadi, E. Demler, and M. Knap, "Far-from-equilibrium field theory of many-body quantum spin systems: Prethermalization and relaxation of spin spiral states in three dimensions," Phys. Rev. X **5**, 041005 (2015), arXiv:1504.05956 [cond-mat.quant-gas].

[20] X.-Y. Song, C.-M. Jian, and L. Balents, "A strongly correlated metal built from Sachdev-Ye-Kitaev models," (2017), arXiv:1705.00117 [cond-mat.str-el].

[21] M. Tsutsumi, "On solutions of Liouville's equation," Journal of Mathematical Analysis and Applications **76**, 116 (1980).

[22] O. Parcollet and A. Georges, "Non-Fermi-liquid regime of a doped Mott insulator," Phys. Rev. B **59**, 5341 (1999), cond-mat/9806119.

[23] T. A. Sedrakyan and V. M. Galitski, "Majorana path integral for nonequilibrium dynamics of two-level systems," Phys. Rev. B **83**, 134303 (2011), arXiv:1012.2005 [quant-ph].

[24] G. Stefanucci and R. van Leeuwen, *Nonequilibrium Many-Body Theory of Quantum Systems: A Modern Introduction* (Cambridge University Press, 2013).

[25] J. Maldacena, S. H. Shenker, and D. Stanford, "A bound on chaos," Journal of High Energy Physics **2016**, 106 (2016), arXiv:1503.01409 [hep-th].

[26] A. A. Patel and S. Sachdev, "Quantum chaos on a critical Fermi surface," Proc. Nat. Acad. Sci. **114**, 1844 (2017), arXiv:1611.00003 [cond-mat.str-el].

[27] A. A. Patel, D. Chowdhury, S. Sachdev, and B. Swingle, "Quantum butterfly effect in weakly interacting diffusive metals," Phys. Rev. X **7**, 031047 (2017), arXiv:1703.07353 [cond-mat.str-el].

[28] J. Engelsöy, "Considerations Regarding AdS_2 Backreaction and Holography," Master Thesis (2017), Department of Theoretical Physics, KTH Royal Institute of Technology, Stockholm.

[29] J. Erdmenger, M. Flory, M.-N. Newrzella, M. Strydom, and J. M. S. Wu, "Quantum Quenches in a Holographic Kondo Model," JHEP **04**, 045 (2017), arXiv:1612.06860 [hep-th].

[30] B. Withers, "Nonlinear conductivity and the ringdown of currents in metallic holography," JHEP **10**, 008 (2016), arXiv:1606.03457 [hep-th].

[31] I. Kourkoulou and J. Maldacena, "Pure states in the SYK model and nearly-AdS_2 gravity," (2017), arXiv:1707.02325 [hep-th].

[32] J. Sonner and M. Vielma, "Eigenstate thermalization in the Sachdev-Ye-Kitaev model," (2017), arXiv:1707.08013 [hep-th].

[33] Y. Gu, A. Lucas, and X.-L. Qi, "Spread of entanglement in a Sachdev-Ye-Kitaev chain," (2017), arXiv:1708.00871 [hep-th].

[34] C.-M. Jian, Z. Bi, and C. Xu, "A model for continuous thermal Metal to Insulator Transition," Phys. Rev. B **96**, 115122 (2017), arXiv:1703.07793 [cond-mat.str-el].